

Implementation of a machine-learned gas optics parameterization in the ECMWF Integrated Forecasting System: RRTMGP-NN 2.0

Peter Ukkonen¹ and Robin J. Hogan^{2,3}

¹Danish Meteorological Institute

²European Centre for Medium-Range Weather Forecasts, Reading, UK

³Department of Meteorology, University of Reading, Reading, UK

Correspondence: Peter Ukkonen (puk@dmi.dk)

Abstract. Radiation schemes are physically important but computationally expensive components of weather and climate models. This has spurred efforts to replace them with a cheap emulator based on neural networks (NN), obtaining large speed-ups, but at the expense of accuracy, energy conservation and generalization. An alternative approach which is slower but more robust than full emulation is to use NNs to predict optical properties, but keep the radiative transfer equations. Recently, NNs 5 were developed to replace the RRTMGP gas optics scheme, and shown to be accurate while improving speed. However, the evaluations were based solely on offline radiation computations.

In this paper, we describe the implementation and prognostic evaluation of RRTMGP-NN in the Integrated Forecasting System (IFS) of the European Centre for Medium-Range Weather Forecasts (ECMWF). The new gas optics scheme was incorporated into ecRad, the modular ECMWF radiation scheme. Using two novel methods to improve accuracy - a hybrid 10 loss function designed to reduce radiative forcing errors, and an early stopping method based on monitoring fluxes and heating rates with respect to a line-by-line benchmark - we train new NN models on RRTMGP k-distributions with reduced spectral resolutions. Offline evaluation of the new NN gas optics, RRTMGP-NN 2.0, shows a very high level of accuracy for clear-sky 15 fluxes and heating rates. For instance, the RMSE in shortwave surface downwelling flux is 0.78 W m^{-2} for RRTMGP and 0.80 W m^{-2} for RRTMGP-NN in a present-day scenario, while upwelling flux errors are actually smaller for the NN. Because closely reproduces radiative forcings for 5 important greenhouse gases across a wide range of concentrations such as 8x CO₂.

To assess the impact of different gas optics schemes in the IFS, four 1-year coupled ocean-atmosphere simulations were performed for each configuration. The results show that RRTMGP-NN and RRTMGP produce very similar model climates, with the differences being smaller than those between existing schemes, and statistically insignificant for zonal means of 20 single-level quantities such as surface temperature. The use of RRTMGP-NN speeds up ecRad by a factor of 1.5 compared to RRTMGP (the gas optics being almost 3 times faster), and is also faster than the older and less accurate RRTMG which is used in the current operational cycle of the IFS.

1 Introduction

Although atmospheric radiation is well understood and very accurate solutions are available, atmospheric models need to settle
25 for a trade-off between the accuracy and cost of radiation computations. This trade-off can be controlled via many factors like the temporal and spatial frequency of computations (Hogan and Bozzo, 2018), simplifying assumptions (e.g. neglecting 3D effects), and spectral resolution (Hogan and Matricardi, 2020). To reduce the latter, most modern radiation schemes use the correlated- k -distribution method (e.g., Goody et al., 1989) since it allows broadband fluxes to be computed with high accuracy using only $O(10^2 - 10^3)$ quadrature points, compared with $O(10^6 - 10^7)$ for line-by-line methods which resolve individual
30 spectral lines in the absorption spectra of atmospheric gases.

Despite this, computations remain expensive enough that many other of the aforementioned approximations need to be made, and still coarse-resolution climate simulations can spend half of the total model runtime on radiation (Cotronei and Slawig, 2020). To make better use of computer resources in an era where computer hardware is becoming more heterogenous, and the gap between hardware peak performance and the performance achieved with typical physics codes is probably increasing even
35 further, machine learning (ML) is a promising way to simultaneously address computational challenges and potentially reduce model uncertainty by representing sub-grid processes more realistically.

Indeed, interest in the use of ML for parameterization of sub-grid processes has been growing, with a particular focus on learning convection or unified physics parameterizations from high-resolution simulations (Rasp et al., 2018; Brenowitz and Bretherton, 2018; Gentine et al., 2018; Brenowitz et al., 2020; Yuval et al., 2021). Using ML specifically for atmospheric
40 radiation has a long history (Chevallier et al., 1998; Krasnopolksy et al., 2008, 2010; Pal et al., 2019; Liu et al., 2020; Roh and Song, 2020; Song and Roh, 2021). These studies trained feed-forward neural networks (FNNs) to emulate a physical radiation scheme, achieving impressive speed-ups typically between 10-100x (although, in many cases relative to outdated or unoptimized codes). Assessing the level of accuracy achieved is difficult in the absence of common datasets, metrics, and comparison against benchmark computations, but reported errors are typically too high to be considered for use in the ECMWF
45 weather forecast model. For instance, shortwave fluxes in Song and Roh (Figure 1, 2021) had root-mean-square-errors (RMSE) of roughly 15 W m^{-2} in offline evaluation against the original scheme. To our knowledge, the ability of FNN-based radiation emulators to compute the radiative forcing due to changes in greenhouse gases has not been evaluated, so such schemes must be considered unsuitable also for climate models until they are shown to do so accurately.

One difficulty in evaluating the FNN approach is that once trained, the models cannot be applied to another dataset (such
50 as that from an intercomparison project) in the likely case that it uses a different vertical grid, since the number of inputs and outputs are fixed and correspond to collapsed and concatenated vertical profiles, and may be large depending on the vertical resolution and the number of gases considered. The high dimensionality in turn implies a difficulty for the models to generalize to e.g. warmer and moister climates given the “curse of dimensionality”. Moreover, to obtain reasonable heating rates, the typical approach has been to predict profiles of heating rates in addition to fluxes at the top-of-atmosphere and surface, as
55 opposed to predicting fluxes and computing heating rates physically. The downside of this approach is that it breaks energy conservation as the fluxes and heating rates are likely to be inconsistent.

An alternative which offers better accuracy, reliability and interpretability at the cost of a smaller speed-up is to use ML only to predict optical properties and couple it to a radiative transfer solver. This may be justified by considering that radiation schemes solve the radiative transfer equation (using the two-stream approximation) to obtain accurate estimates of broadband radiative fluxes, after having first computed spectral optical properties of gases, clouds and aerosols, ideally in separate modules (Fig. 1, Hogan and Bozzo, 2018). In contrast, parameterizations of other processes are often based more on empirical relationships and simplified theories (Wang et al., 2022). The computation of optical properties (which control the absorption, emission and scattering of radiation) within radiation schemes are likewise data-driven, as they rely on look-up-tables. This is arguably a much easier and more suitable problem for neural networks than computing radiative flows from one vertical level to the next, especially for feed-forward networks which do not structurally incorporate the vertical dependencies of the latter.

FNNs were consequently developed to emulate the gas optics parameterization RRTM for General circulation model applications—Parallel (RRTMGP) (Pincus et al., 2019) in two different studies, which found speed-ups of 2–6x compared to the original code (Ukkonen et al., 2020; Veerman et al., 2021). In the former study the NN gas optics was combined with a refactored radiative transfer solver to speed up the entire radiation scheme (without cloud or aerosol optics) by a factor of 1.8–3.5. Recently, Ukkonen (2022a) compared different emulation strategies for shortwave radiation, and found that using NNs for gas optics hardly affected accuracy at all, whereas replacing the entire scheme with FNNs was the fastest but also least accurate approach, with heating rates computed from fluxes having a RMSE of 1.35 K day^{-1} . An interesting middle-ground was found in using bidirectional recurrent neural networks, which structurally resemble physical computations, to emulate the full radiation scheme. This produced far more accurate fluxes (RMSE of $1\text{--}1.5 \text{ W}^{-2}$) and heating rates (RMSE 0.16 K day^{-1}) than FNNs while offering a smaller, but still appreciable speedup.

While the recent studies show that gas optics emulation is at this point more suitable for operational implementation than replacing the full radiation scheme, not least due to inherently better generalization (e.g. to arbitrary vertical grids), the evaluations were based on offline radiation computations (Ukkonen et al., 2020; Veerman et al., 2021; Ukkonen, 2022a). As the offline accuracy does not necessarily reflect its performance when coupled with other components (Liu et al., 2020), the NN version of RRTMGP (Ukkonen et al., 2020) is in this work integrated into the ecRad radiation scheme used in the Integrated Forecasting System (IFS), which is a global numerical weather prediction model developed at the European Centre for Medium-Range Weather Forecasts (ECMWF). New NN models are trained on reduced-resolution RRTMGP k -distributions that recently became available, which have around the same number of k -terms as the older RRTMG scheme that is used operationally in the IFS. Free-running simulations are then performed in order to test the generalization and accuracy of the NNs in a prognostic setting. In the context of wider literature on ML-based parameterizations, our focus on gas optics represents a more typical model development approach focusing on modules, and aims for immediate application in numerical weather prediction (NWP) and climate models. On the other hand, the gas optics scheme plays a very central role in climate models as pointed out by Hogan and Matricardi (2022) and is often computationally a significant part of the full radiation scheme (Hogan and Bozzo, 2018; Ukkonen et al., 2020).

The structure of the paper is as follows: Section 2 briefly describes the ecRad and RRTMGP-NN codes, and the implementation of RRTMGP-NN in ecRad. Section 3 provides an overview of the machine learning methodology, which has been refined

to reproduce radiative forcings with respect to individual gases more accurately. The results are then presented in Section 4, consisting of an offline evaluation, and a prognostic evaluation where the impact of the new gas optics schemes (RRTMGP and RRTMGP-NN) on model climate is determined using a small ensemble of year-long IFS simulations.

95 2 Codes

2.1 ecRad

ecRad is a radiation scheme developed at ECMWF and used operationally in the IFS since 2017 (Hogan and Bozzo, 2018). It is highly configurable with multiple options for gas optics, cloud optics, aerosol optics, and radiative transfer solvers which represent cloud heterogeneity in different ways and support various cloud overlap assumptions.

100 2.2 RRTMGP

RRTMGP is a recent gas optics scheme with a correlated k -distribution that is based on state-of-the-art spectroscopy. It is part of a freely available toolbox, RTE+RRTMGP, that couples it to a radiative transfer solver (RTE). The radiation scheme seeks to balance accuracy, efficiency and flexibility and both the code and data continue to evolve (Pincus et al., 2019). The original RRTMGP k -distributions have a relatively large number of k -terms, also known as g -points: 224 in the shortwave (SW) and 256 in the longwave (LW), corresponding to 16 in each SW and LW band, of which there are 14 and 16 respectively. Recently, reduced k -distributions with half the number of g -points (112/128) have been generated from the full distributions. This was done using the same approach as in the evolution from the RRTM scheme (Mlawer et al., 1997) to its reduced-resolution version designed for GCMs, RRTMG (Iacono et al., 2000), namely by iteratively combining neighboring g -points while attempting to minimize a cost function that includes fluxes, forcing, and heating rates (R. Pincus and E. Mlawer, personal communication, 105 May 24, 2022). The reduction in g -points was similar in both cases; RRTMG, which is used operationally in the IFS, has 112/140 g -points.

As the number of g -points gives the number of pseudo-monochromatic radiative transfer calculations, it largely determines the cost of the whole radiation scheme. The NNs developed in this paper are therefore based on the new reduced k -distributions (“Reduced-RRTMGP”), and not the k -distributions with higher spectral resolution (“Full-RRTMGP”).

115 2.3 RRTMGP-NN and implementation in ecRad

RRTMGP-NN is a neural network version of RRTMGP described in Ukkonen et al. (2020), available with a refactored version of the RTE solver which has columns as the outermost dimension (in terms of memory location) instead of g -points. The modified radiation scheme is referred to as RTE+RRTMGP-NN and like the original code, it is written in modern Fortran. The simple yet efficient NN kernel is based on BLAS routines for batched inference, exploiting the lack of vertical and horizontal 120 dependencies in gas optics computations. The code can also be run on GPUs, in this case NVIDIA cuBLAS is used for the matrix multiplications and OpenACC directives are wrapped around the remaining computations. (While efficient, the speed

advantage over version 1.5 of RTE+RRTMGP is actually much smaller on GPU than CPU, as shown in section 3.2 of Ukkonen, 2022b). The underlying structure of RRTMGP and RRTMGP-NN is loosely sketched out in Fig. 1 to demonstrate why the latter is more efficient. For the purpose of clarity, the computation of optical properties in RRTMGP has been simplified in the diagram: for each band, the code actually computes the absorption by 1-2 “major” gas species by 3D interpolation in temperature, pressure and η , relative abundance of the two major species (Pincus et al., 2019). The contribution from less important “minor” gases are computed separately using 2D interpolation for each minor gas in the band; therefore, a given band is written to several times. The NN gas optics instead predicts all spectral points simultaneously given an input matrix containing all gases.

RRTMGP-NN previously loaded models from ASCII files like the Neural-Fortran code (Curcic, 2019) that it is built upon. We have refined the code so that models are loaded from netCDF files, which contain not only the weights and activation functions, but also coefficients used for scaling inputs and outputs, as well as metadata about the training data. These files could in the future be expanded to replace the k -distribution files in their entirety, keeping relevant metadata and the look-up-table coefficients used to compute Planck sources from Planck fraction and temperature.

We now briefly describe the integration of RRTMGP into ecRad. The goal was to avoid larger changes in ecRad. However, since RTE+RRTMGP makes heavy use of Fortran derived types to specify e.g. gas concentrations and optical properties, use of existing RRTMGP interfaces would imply a significant amount of array copying to communicate between ecRad and RRTMGP derived types. Large changes in RRTMGP are not desirable either, because they reduce maintainability of the gas optics code.

With these conflicting goals in mind, a balance was sought with non-intrusive changes in both codes, but prioritizing minimal changes in ecRad. Firstly, the refactored radiation scheme with neural networks, RTE+RRTMGP-NN, was implemented instead of the reference gas optics code in order to make direct use of existing NN code. This has the advantage that RTE+RRTMGP-NN uses the same dimension order as ecRad with optical properties having g -points innermost and columns as the outermost dimension, removing the need for array transposes which can be a computational bottleneck (Ukkonen et al., 2020). While the NN fork of RTE+RRTMGP is currently only maintained by one person, the code is very similar to RTE+RRTMGP. The k -distributions are loaded from netCDF files which can be copied over as new ones are made available in the main repository.

The RRTMGP(-NN) package was then added as an ecRad subdirectory, with some small changes to remove the dependence on RTE. The source code of RRTMGP-NN is kept separate: it does not use any of the ecRad modules. Instead, new interfaces were written for RRTMGP-NN for easy interoperability with ecRad and avoiding array copying. For instance, the new interface for the longwave (*gas_optics_int_ecRad*) replaces the derived type arguments of the original RRTMGP interface, containing optical properties and Planck sources, with explicit shape arrays used in ecRad. The computational kernels remain the same, as in original RRTMGP they do not use derived types. In ecRad, another interface then prepares the RRTMGP-NN gas concentrations (columns outermost) by transposing the ecRad gases (columns innermost) and calls *gas_optics_int_ecRad* (longwave) and *gas_optics_ext_ecRad* (shortwave). ecRad has similar interfaces to the RRTMG and ecCKD (Hogan and Matricardi, 2022) gas optics schemes. The overhead from transposing the gases and thermodynamic arrays is very small. The k -distributions and NN models are stored in the ecRad “config” derived type in order to avoid introducing new arguments to the main interface.

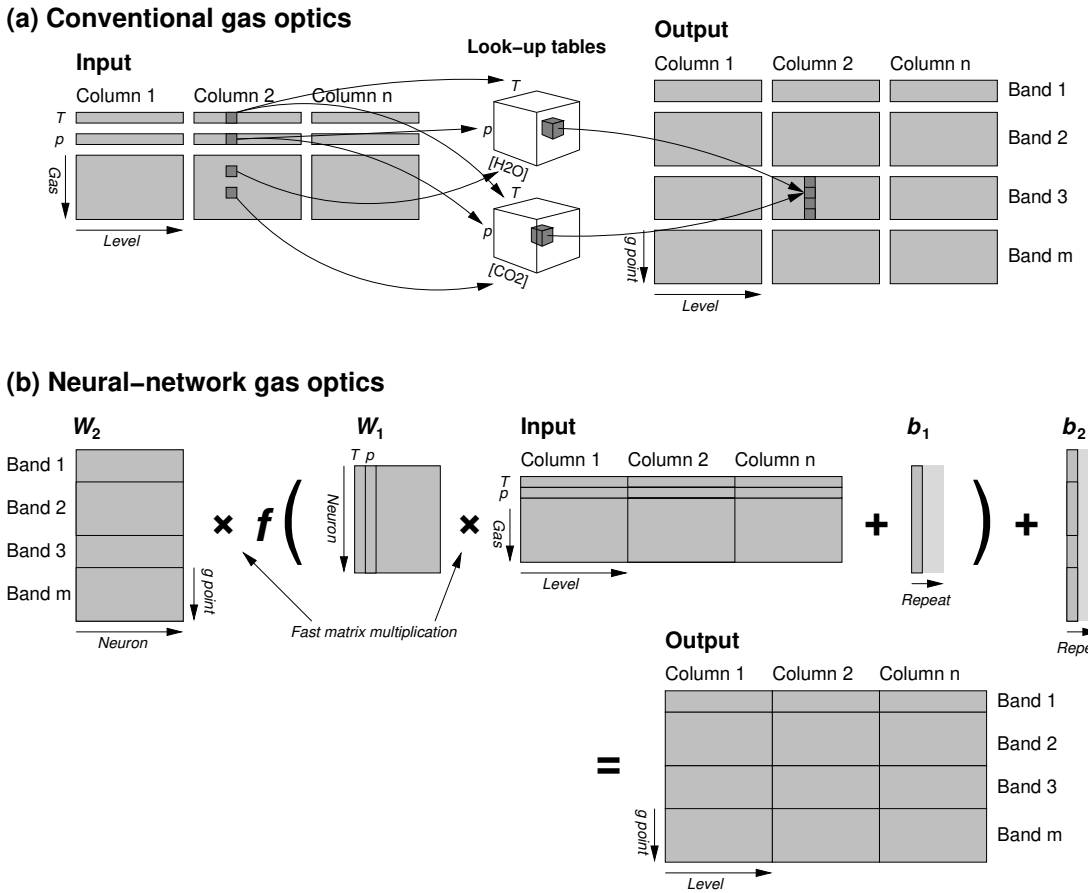


Figure 1. Schematic illustrating the data flow in a structure of (a) a conventional gas-optics scheme such as RRTMGP, and (b) RRTMGP-NN. For a given band, RRTMGP makes several calls to interpolation kernels to compute gas-specific contributions to optical properties, accounting for temperature (T) and pressure (p) dependencies, as well overlap of major gases in the band. These kernels loop over the g -points in a single band, of which there are only 1-12 in the reduced k -distributions, leading to poor vectorization. The steps are repeated for each vertical level and column. The NN (b) achieves better performance i) by predicting a vector containing all g -points from a vector containing T , p , and the mixing ratios of all gases (treating gas interactions implicitly by the NN), and ii) batching the computations for multiple atmospheric levels and columns by expressing the core NN computations as matrix-matrix multiplications (between weights W and input matrices) that are delegated to a BLAS library. For each hidden NN layer, this is followed by addition of biases b and transformation by a non-linear activation function $f(x)$. The schematic shows a network with only one hidden layer; in this study two hidden layers are used.

3 Machine learning

In training NNs to emulate RRTMGP, we use a similar methodology as in Ukkonen et al. (2020), where detailed offline evaluation against line-by-line computations suggested a similar level of accuracy in overall fluxes and heating rates as the

original scheme, despite using fairly simple NN models with two hidden layers and 16-48 neurons in each hidden layer.

160 Various aspects of the methodology are refined from the previous paper as described below.

3.1 Data

We use similar training data as in Ukkonen et al. (2020), in which a diverse and extensive data set was prepared from several sources, including atmospheric profiles used in previous radiation studies, as well as data from future climate experiments and a reanalysis. These initial data sets were synthetically supplemented, or extended, by varying greenhouse gas concentrations both

165 manually and by using Hypercube sampling. The data in this study differs from Ukkonen et al. (2020) principally in two ways.

Firstly, data provided by the Radiative Forcing Model Intercomparison Project (RFMIP, Pincus et al., 2016), comprising of 100 profiles and 18 perturbation experiments, now serves as an independent validation dataset used for early-stopping (section 3.3) instead of training. These profiles were designed to assess global mean clear-sky errors in instantaneous radiative forcing and should be well-suited as an out-of-sample test for our purposes. Secondly, a different dataset based on the CAMS reanalysis

170 (Inness et al., 2019) is used. The new CAMS data uses the same approach as the IFS and the Correlated k -distribution Model

Intercomparison Project (CKDMIP, Hogan and Matricardi, 2020), where only nine gases are considered, but the radiative forcing of many minor greenhouse gases is represented by artificially increasing the concentration of CFC-11 (Meinshausen et al., 2017). The height dependence of these gases is represented, and other RRTMGP gases are set to zero. (Neither of these generally applies to the remaining training data, where all minor RRTMGP gases are included, but as scalar concentrations).

175 The reanalysis profiles are designed to encompass the variability in present-day atmospheric conditions, with the following steps taken to increase variance and capture extremes. Starting from an initial pool of roughly 164 000 profiles spanning global

reanalysis data from 2008 and 2017 and interpolated to a 320 km resolution equal-area grid (Ukkonen, 2022a), 1000 profiles were drawn. Of these, 17 were selected to contain the minimum and maximum of temperature, humidity and ozone at different pressure levels (a total of 9 variables) in the whole dataset, similarly to Hogan and Matricardi (2020). Another 486 profiles

180 were selected by constructing $k = 81$ k -means clusters which are clustered in the 9 dimensions represented by the variables

in the previous step. From each cluster, which the k -means algorithm ensures are as different to other clusters as possible, 6 random profiles were selected. The remaining roughly 500 profiles were randomly drawn from the entire dataset minus ones already chosen. Vertical profiles selected by the minimum-maximum, semi-random and random method are depicted in Fig. 2.

The 1000 CAMS profiles were then expanded into 42 experiments or scenarios where CO₂, CH₄, N₂O, CFC11-eq and

185 CFC12 are varied similarly to Hogan and Matricardi (2020) where the concentration of gases were individually varied across

a large range, keeping other gases constant, except for CO₂, CH₄ and N₂O which were also perturbed in pairs to account for the overlap in their absorption spectra. The $1000 \times 42 \times 60$ (layers) ≈ 2.5 million samples make up roughly 47% of the 5.42 million total training samples. The remaining parts comprise i) end-of-century CMIP6 data corresponding to a high-emissions scenario, ii) profiles from the “mean-maximum-minimum” CKDMIP dataset, and iii) 42 profiles used for tuning RRTMGP; all

190 of which were expanded into up to hundreds of experiments as described in Ukkonen et al. (2020). The data is summarized in

Table 1.

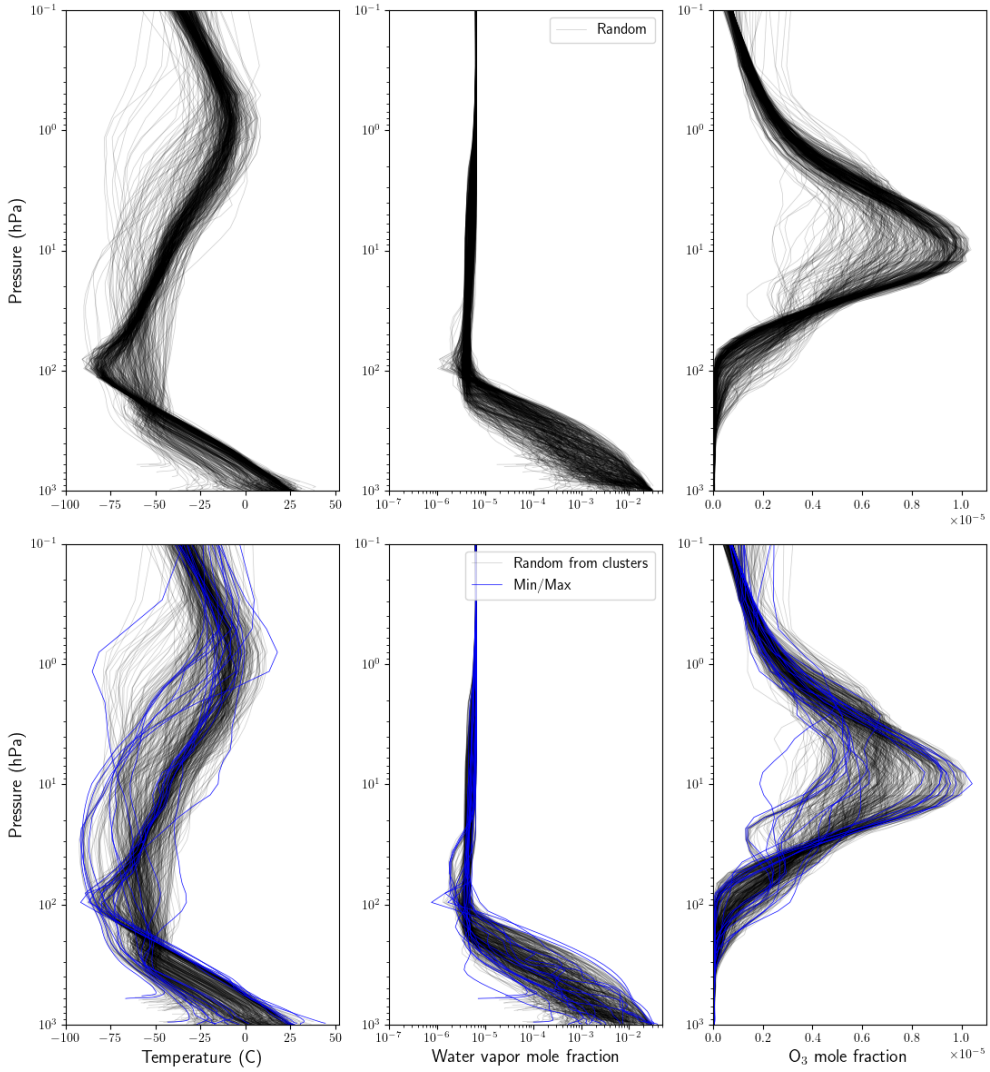


Figure 2. Vertical profiles of temperature, water vapor and ozone selected from the CAMS data as described in Sect. 3.1. The top panel shows 486 random profiles (black), and the bottom panel shows 486 profiles drawn from k-means clusters (black) and 17 that were selected to sample minimum and maximum values (blue).

3.2 Choice of inputs and outputs

Our RRTMGP emulator predicts layer-wise optical properties from an input vector which contains gas mixing ratios, temperature, and log-pressure. The NNs take as input all the RRTMGP gases and output all g -points, which results in better computational intensity and efficiency than computing one band at a time, and the contributions from minor gases one gas at a time, as is done in the look-up-table (LUT) kernels in RRTMGP (Ukkonen et al., 2020). In the shortwave (SW), the NN out-

Table 1. Different subsets of the gas optics training data. The original data contained only *profiles* (or columns), and were extended to sample different greenhouse gas scenarios and/or temperature ranges in different *experiments*. For further information and more detail about the last three datasets the reader is referred to section 3.2 of Ukkonen et al. (2020).

Dataset / Original source of profiles	Application	Experiments	Profiles	Layers	Total samples $\times 10^6$
CAMS reanalysis	NWP, climate	42	1000	60	2.52
CMIP6	Climate	200	420	19	1.596
Garand et al. (2001)	NWP, climate	322	42	42	0.568
CKDMIP-MMM (Hogan and Matricardi, 2020)	NWP, climate	58	243	52	0.733

puts are absorption and Rayleigh cross-sections, while the longwave (LW) predictands are absorption cross-section and Planck fraction. Here, cross-sections refers to optical depth divided by the number of dry air molecules in a layer N . This allows generalization to arbitrary vertical grids, since optical depths are obtained in a separate step by multiplying the cross-sections with N . Meanwhile, *Planck fraction* is the fraction of a band's total Planck function that is associated with each LW g -point, obtained by 3D interpolation in the original code. Like in RRTMGP, this is multiplied with the band-integrated Planck function at a level or layer (interpolated from a LUT using the temperature of that level/layer) to get the Planck function for each LW g -point. This retains a small LUT interpolation, but simplifies the NN model by requiring only ng outputs, instead of $3 \times ng$ to directly predict the Planck functions used in reference RRTMGP, or $2 \times ng$ to get the Planck functions in RRTMGP-NN. (The original code has one Planck variable for each layer and two for each layer interface, the upward and downward emission, whereas RTE+RRTMGP-NN has one for each layer and layer interface. ecRad only uses one Planck function, defined at layer interfaces). Reducing the number of NN outputs can decrease model complexity and runtimes, since most of the floating point operations occur in the final NN layer given $N_{gpt} > N_{neurons} > N_{inputs}$. However, in this work a single LW model is used which predicts both absorption cross-sections and Planck fractions as one big vector. This may not be the fastest approach but has the benefit of easing the optimization procedure described in the next section.

In addition to predicting cross-sections instead of optical depths, to obtain good results with less complex models it is useful to pre-process both inputs and outputs. Firstly, the distributions of all outputs and some inputs were made more uniform by taking their N-th square root (a weaker form of log-scaling, see Table 1 in Ukkonen et al., 2020), and afterwards the inputs are scaled to the 0-1 range and outputs are scaled to have roughly zero mean and unit variance by using a variant of standardization that preserves correlations between different outputs (Ukkonen et al., 2020).

3.3 Optimizing for fluxes when predicting optical properties

Training gas optics ML models presents a tuning challenge, as the variables we ultimately care about are not optical properties but radiative fluxes and heating rates - outputs from the solver. We previously found it relatively easy to develop gas optics NNs which upon implementation in the radiation code result in low mean errors in fluxes and heating rates, but difficult to obtain accurate radiative forcings at the top-of-atmosphere or surface with respect to changes in the concentration of individual gases, especially minor ones (Ukkonen et al., 2020). The problem is likely to stem from predicting aggregated optical properties,

instead of computing the contribution from minor gases separately (as is usually done in k -distributions), which is more efficient but leads to major gases dominating the loss function. Mostly accurate radiative forcings for CKDMIP gases were ultimately obtained via a time-consuming, iterative process where new models were continuously trained, evaluated, and the training data 225 expanded. In this work we have attempted to automate the optimization with regards to fluxes, heating rates and forcings to at least some extent by adding two new techniques to the training methodology.

Firstly, errors in fluxes and heating rates were monitored during training. While these metrics cannot easily be used for 230 optimizing the NN weights, they can be used as a criteria to know when to stop training (*early-stopping*), or to optimize NN hyperparameters. Therefore, a Python training program was written where at the end of every epoch, the NN models are saved to a file, and the Fortran radiation program is called with the new model, passing the location as a command-line-argument. The Fortran program runs RTE+RRTMGP-NN on a validation dataset, and writes some error metrics to standard output, which 235 are finally read by the training program. For validation we used the RFMIP dataset consisting of 100 profiles and 18 different perturbation experiments, which allowed computing radiative forcing errors with respect to CH₄, N₂O, and total forcing errors with respect to all RRTMGP gases. In addition, a benchmark line-by-line solution was available for this data, meaning that the 240 total (parameterization) error can be determined instead of only emulation (NN) error. Our goal was to develop NNs that have a similar level of accuracy as RRTMGP; that is, emulation errors should be smaller than parameterization errors. The error metrics were normalized by the RRTMGP values, so that a value of one indicates the same level of performance as RRTMGP, and larger values indicate worse performance. An overall "radiation error" was computed by taking the RMS value of a total of 8 metrics which differ slightly for the longwave and shortwave (Table 2; the choices were ad-hoc but emphasize heating rate errors in the SW and radiative forcing errors in the LW). This overall metric was used in the early stopping criteria and the model weights from the best epoch (a minimum in the metric) were saved.

Table 2. Metrics that comprise the overall "radiation error". TOA = top of atmosphere, IRF = instantaneous radiative forcing, "future-all" = a radiative forcing experiment with perturbed atmospheric conditions in addition to greenhouse gas concentrations.

Metric	Longwave	Shortwave
MAE Heating rate	X	X
MAE Heating rate (present-day)	X	X
MAE Heating rate (preindustrial)		X
MAE Heating rate ("future-all")		X
Bias surface downwelling flux		X
Bias TOA upwelling flux	X	
Bias TOA IRF (present-day - preindustrial)	X	
Bias TOA IRF (future - present-day)	X	
Bias TOA IRF (future - preindustrial)		X
Bias surface IRF (future - preindustrial)	X	X
Bias surface IRF CH4 (present-day - preindustrial)	X	X
Bias surface IRF N2O (present-day - preindustrial)	X	

Secondly, a custom loss function was devised to minimize the error in the difference in y associated with different perturbation experiments, in addition to mean-squared-error of y , where y are the scaled NN outputs. The new loss function indirectly measures radiative forcing errors (albeit weakly due to a non-linear dependence between spectral optical properties and broadband fluxes) and has the form:

$$loss = \alpha \sum_{i=1}^N (y_i - \hat{y}_i)^2 + (1 - \alpha) \sum_{\substack{i=1 \\ i \text{ odd}}}^N \left((y_{i+1} - y_i) - (\hat{y}_{i+1} - \hat{y}_i) \right)^2,$$

where y and \hat{y} are the target and NN output vectors, respectively, and α is a coefficient that was set to 0.6 for LW and 0.2 for SW after testing a few different values and finding that these seemed to give a reasonable trade-off between heating rate errors and radiative forcing errors. The second term measures the error in the difference in y between different perturbation experiments if the data is organized so that adjacent samples (of a total N training samples) correspond to different experiments but the same columns and vertical layers, which was achieved by transposing the data so that the experiment dimension is innermost. In addition, the perturbation experiments must be designed and arranged in memory so that neighboring indices relate to the goal, which was minimizing the TOA and surface forcing errors of individual gases (for instance, a pair of adjacent experiments could be pre-industrial and present-day N₂O). Therefore, RFMIP-style experiments such as present-day 255 versus future concentrations of all greenhouse gases, or 8X CO₂ versus preindustrial CO₂, should be avoided, as they can easily dominate the error compared to varying the concentration of minor greenhouse gases (which was the challenge to begin with). This requirement was only partially fulfilled since we wanted to make use of existing data. Though rather convoluted, and requiring bespoke data, the approach does reduce forcing errors (Fig. 3).

In the end, there was still a substantial random element in obtaining good results, and several models were trained before 260 settling on the final models (based on errors with respect to training data, and not the independent offline evaluation, which was only performed once). To obtain a satisfactory LW model the early-stopping criteria was loosened to 70 consecutive epochs of no improvement. In addition, increasing the number of hidden neurons from Ukkonen et al. (2020) seemed to improve results (the number of model parameters remains similar; this is explained by the number of g -points being roughly half of the previous k-distributions). The final LW model has two hidden layers with 64 neurons in each layer, and the SW models have 265 two hidden layers with 32 neurons in each layer. All models use the “softsign” activation function and were trained using the Adam optimizer, a batch size of 2048 and learning rate of 0.01 as in our previous paper.

Future studies could explore directly minimizing flux and forcing errors when training NN-based gas optics models. Doing this via gradient descent optimization would require differentiating the radiative transfer solver to obtain the derivative of fluxes with respect to changes in optical properties (and NN weights), which should be possible using automatic differentiation tools 270 like the Python library JAX (Bradbury et al., 2018) if the radiative transfer code was re-written in the supported language or API (JAX, for instance, has an API based on NumPy). Finally, we note that while ecRad uses g -points innermost, the NN models themselves are agnostic to whether the batch dimension is innermost or outermost, and so in principle could be used by a radiation scheme with columns innermost. (An inference kernel for such a case, `output_sgemm_flat_byrows`, can be found in RTE+RRTMGP-NN within `neural/mod_network.F90`).

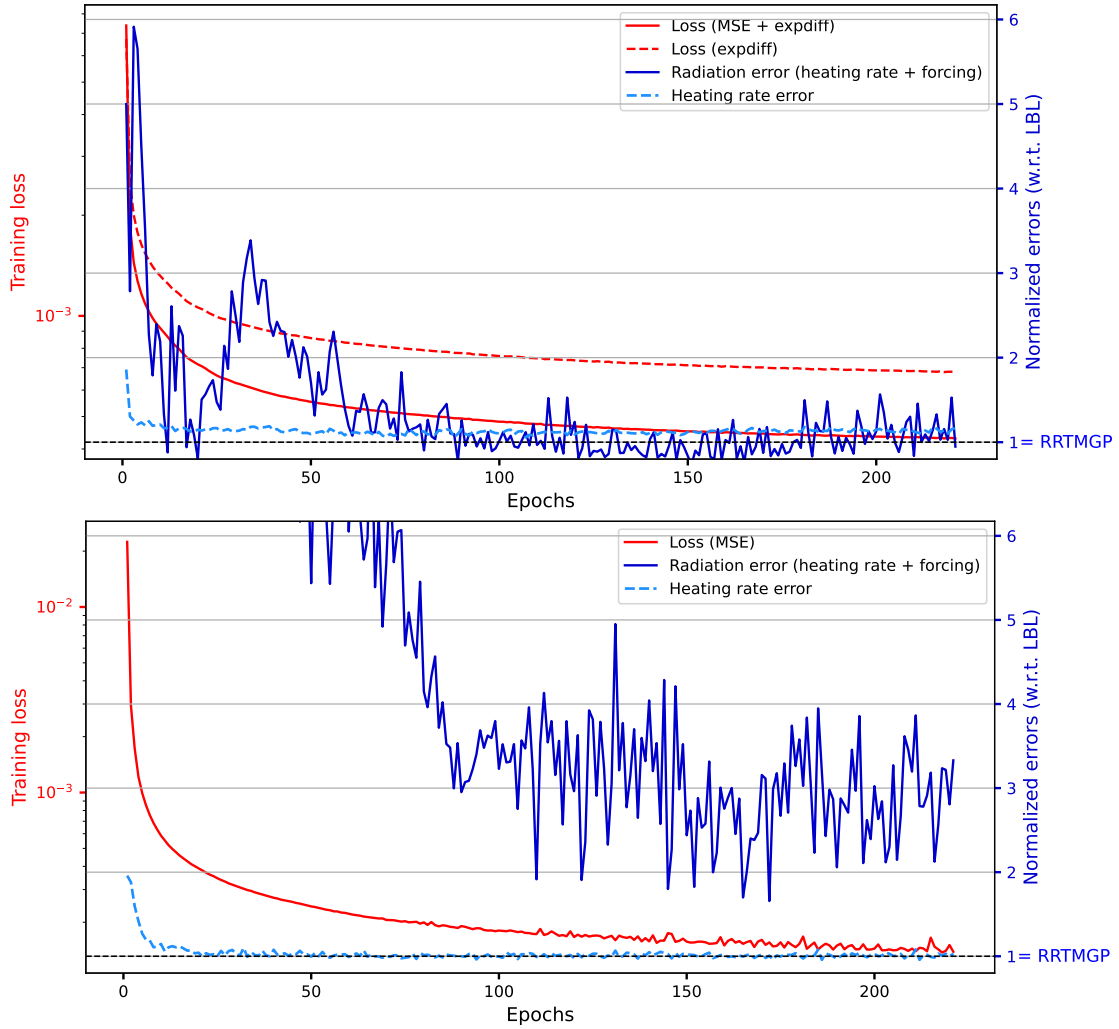


Figure 3. Monitoring of heating rate error (dashed cyan line, given by the mean of the LW heating rate metrics in Table 2), and the total radiation error (solid blue line, given by the RMS of all the LW metrics listed in Table 2) when training the final LW gas optics model using a hybrid loss function and early stopping (top), and training for the same number of epochs with a regular loss function (bottom). The monitored errors (right axis) are computed using the RFMIP data with respect to line-by-line results and normalized by the RRTMGP value. Also shown are the training losses (solid and dashed red lines). The larger radiation error when not using the hybrid loss function (b) was largely due to a single metric, the surface radiative forcing of N₂O (not shown).

275 4 Results

In this section we evaluate the accuracy and speed of ecRad with different gas optics schemes (RRTMGP, RRTMGP-NN, and the older RRTMG scheme) in both an offline and online setting. The results were obtained using an optimized development version of ecRad which refactors the Tripleclouds (Shonk and Hogan, 2008) and SPARTACUS (Hogan et al., 2016) solvers

for better efficiency and includes the new RRTMGP(-NN) gas optics. One change is that reflectances and transmittances are
280 computed in the same numerical precision as the rest of the model (in the operational version of ecRad, these two-stream computations are always performed in double precision), which improves the single-precision performance of all solvers in ecRad. The updated solvers also improve efficiency by batching the reflectance-transmittance computations for multiple vertical levels. The optimizations, to be described in a forthcoming paper, have a negligible impact on fluxes and heating rates while making Tripleclouds significantly cheaper, and thus increase the share of the gas optics in ecRad’s total runtime.

285 The prognostic evaluation and offline timings were obtained with an ecRad configuration close to operational IFS Cycle 47r3, which is similar to the 46r1 settings given in Table 2 of Hogan and Bozzo (2018), except for replacement of the pure exponential cloud overlap assumption with “exponential-random” whereby an vertically contiguous cloud layers are partially correlated but cloud layers separated by clear sky are randomly overlapped. Furthermore, instead of the McICA solver we use Tripleclouds due to the latter being noise-free and a likely candidate for operational use in a near-future cycle.

290 It should be noted that the RRTMGP results were not produced using the original RTE+RRTMGP package, which uses two Planck source functions for half-levels which are then combined into one, and the LW results (Figures A1-A4 in Appendix A), and could be very slightly impacted by the simpler computation of Planck source in RRTMGP-NN. For simplicity the RRTMGP-NN code configured with look-up-tables and not NNs is hereafter referred to as RRTMGP.

4.1 Speed-up

295 The runtime of ecRad with different gas optics schemes was evaluated offline using 10,000 input profiles that were randomly sampled from a global snapshot saved from a high-resolution IFS run. Figure 4 shows timing results obtained on a single node of the new ECMWF AMD-based supercomputer in Bologna, to which EMCWF’s operational forecast migrated in October 2022.

300 With Reduced-RRTMGP, the runtime of ecRad is slightly higher than with RRTMG due to the new gas optics scheme (shown in light blue) being more expensive. The older gas optics module is faster by a factor of 1.41 despite the similar spectral resolution. The poor efficiency of RRTMGP is explained by short inner loops in the LUT code that iterate over the number of g -points in a band (which is only 1-12 for the smaller k -distributions), leading to poor vectorization. However, speed is improved drastically with the NN version of Reduced-RRTMGP, which is roughly 2.87 times faster than the LUT-based code, and 2 times faster than the operationally used RRMTG scheme. The resulting speedup in the full radiation scheme
305 is 1.48x and 1.29x compared to RRTMGP and RRTMG respectively.

We note that the speed-up achieved with RRTMGP-NN is heavily influenced by many factors, such as the hardware and software platform (especially the performance of the BLAS library) but also the number of gases included. While our new RRTMGP-NN models support all of the 11 minor greenhouse gas species in RRTMGP, here only the reduced set of gases (with CFC-11-equivalent) is used as input in ecRad and evaluated (remaining gases were set to zero in the NN inputs). Including a
310 large number of greenhouse gases would slow down reference RRTMGP where the kernel has a loop over minor gas species, whereas the runtime of RRTMGP-NN would hardly be affected, improving the speed-up further. Indeed, one benefit of our NN

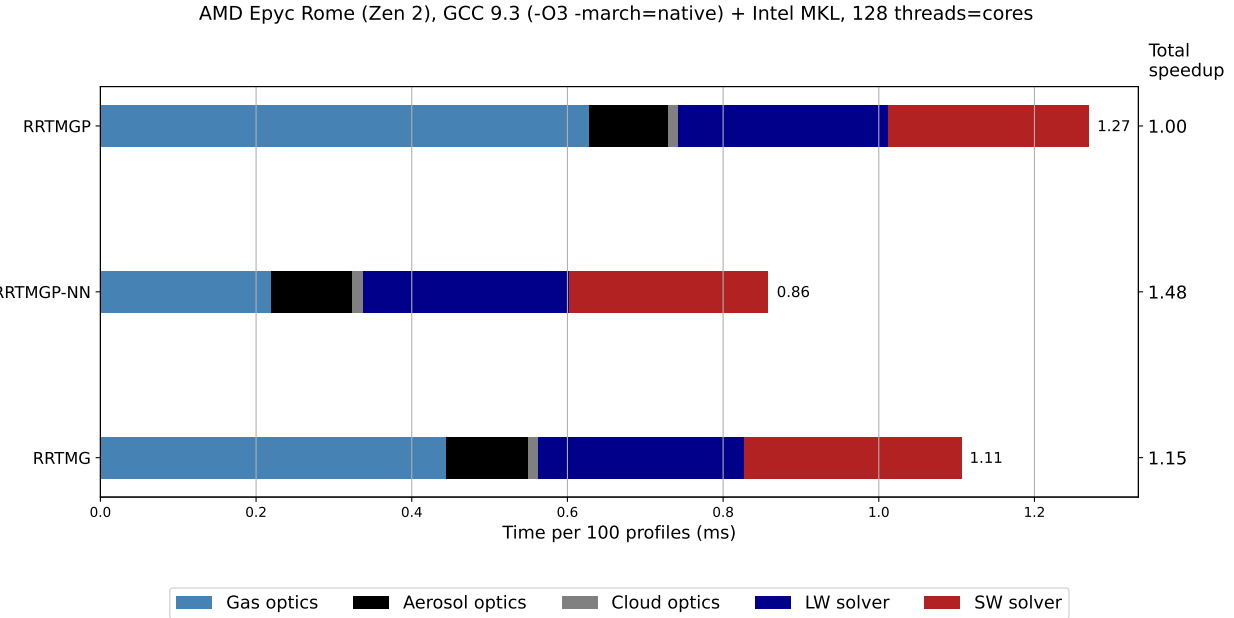


Figure 4. Runtime of ecRad in single precision per 100 atmospheric profiles with 128 levels (x-axis) when combining different gas optics (y-axis) with the TripleClouds solver, broken down into components. Three gas optics schemes are compared: RRTMGP with reduced spectral resolution (112 SW and 128 LW g -points), its neural network version (RRTMGP-NN), and the older RRTMG scheme with 112 (SW) and 140 (LW) g -points. The 10,000 original columns with 137 vertical levels were repeated 4 times into 40,000 columns that were blocked in an OpenMP loop in which ecRad is called (blocking the derived type arguments and using a block size of 8 columns to reflect IFS use). Computations were repeated 10 times in an outermost loop, and furthermore the program was run 3 times, with the fastest result saved. The component runtimes are means of per-thread values reported by GPTL, but normalized to add up to the total time spent in the OpenMP loop (annotated to right of the bars), which was incrementally higher than the sum of section means. The speed-up relative to RRTMGP is shown to the right of the bar plot. Platform: 2x 64-core AMD EPYC 7H12 CPUs, GNU Fortran compiler version 9.3 and Intel MKL library 19.0.5 (used for general matrix-matrix multiplication (GEMM) in RRTMGP-NN).

approach is that it can account for many minor gases essentially for free in a computational sense (although, not necessarily accurately, and in the next section we do not evaluate radiative forcings with respect to non-IFS gases).

4.2 Offline evaluation

315 Independent validation of the NN gas optics models was carried out by using data and tools from CKDMIP (Hogan and Matricardi, 2020). The data are from the ‘Evaluation-1’ dataset, which was not used for training. The accuracy of the new RRTMGP-NN SW model, relative to a line-by-line benchmark, is first shown in Fig. 5 for the present-day scenario. The NN has almost identical accuracy as the Reduced-RRTMGP scheme it was trained on (Fig. 6), particularly in terms of heating rates, which in both cases have an RMSE of only $0.056\text{--}0.057\text{ K d}^{-1}$ below 4 hPa. Surprisingly, the bias and root-mean-square errors

320 in upwelling fluxes are actually smaller when using NNs. Results using the other CKDMIP concentration scenarios (Glacial Maximum, Preindustrial, and Future) are not presented here but are very similar, with the NN gas optics resulting in better upwelling fluxes but similar heating rates.

325 In general, the close emulation of RRTMGP was already demonstrated in Ukkonen et al. (2020) and so the remaining results are not discussed in detail, but the LW results for present-day and future scenarios are provided in Appendix A (Figures A1-A4).
330 The improvement in upwelling fluxes (but not heating rates) is even more pronounced in the longwave, with RRTMGP-NN resulting in 40-50% lower biases in TOA upwelling flux than the original scheme for the various concentration scenarios. The result is therefore probably not a fluke, but attributable to using early-stopping based on a line-by-line benchmark. The exact mechanism for this is unclear, but it's plausible that the NN fits to physically correct signals in the data before it fits to reproduce RRTMGP errors with respect to LBL (or, the result is indeed a fluke; heating rate errors are slightly worse than for RRTMGP). The most notable difference to our earlier paper is that the top-of-atmosphere and surface forcings with respect to N₂O, CFC11 and CFC12 have been improved with the help of a hybrid loss function and are now excellent (Fig. 7). We note that the new Reduced-RRTMGP *k*-distributions with 112 (SW) and 128 (LW) *g*-points seem to trade only a little accuracy for nearly halving the cost of the radiation scheme, compared to the original *k*-distributions with almost double the spectral resolution (<https://confluence.ecmwf.int/display/CKDMIP>). The only major degradation is in longwave heating rates in the mesosphere, with reduced-RRTMGP introducing a considerable warming bias in the mid-mesosphere.

4.3 Prognostic evaluation

340 We now describe results from a prognostic evaluation of RRTMGP-NN and RRTMGP using 1-year free-running simulations with the IFS model. The model simulations consisted of four atmosphere-ocean coupled simulations 13 months long initialized on 1 August of the years 2000, 2001, 2002 and 2003. After a 1-month spin-up for each simulation, the remaining 12 months were averaged over each simulation. This configuration is very similar to that used in section 5 of Hogan and Bozzo (2018) to evaluate the impact of changes to the radiation scheme; the simulations are long enough to capture fast atmospheric and land-surface processes that respond to changes in the treatment of radiative transfer, but short enough that the response is not significantly affected by the longer-term changes to ocean circulation. The one-year forecast length also matches the longest operational forecast length used in ECMWF's seasonal forecasts. The model configuration was as in operational IFS model 345 cycle 47r3 except for the use of the Tripleclouds rather than McICA solver. The horizontal resolution was T_{CO}199 (around 60 km) and 137 vertical levels were used. The radiation scheme was called every hour.

350 The impact of different gas optics schemes on annual-mean temperature from the surface to the lower mesosphere is shown in Fig. 8. Because RRTMGP is not, to our knowledge, routinely tested in single precision, both single and double precision runs were performed with both Reduced-RRTMGP and Full-RRTMGP. The NN version of Reduced-RRTMGP was only tested in single precision (internally, RRTMGP-NN always uses SP, as higher numerical precision does not benefit NNs). In general, larger differences between the runs are only seen in the mesosphere and upper stratosphere, which are very sensitive to heating-rate differences. Comparison against a reference dataset based on the Microwave Limb Sounder (MLS) instrument above 20 hPa, and ERA5 reanalysis data below this level is depicted in Fig. 8 (b) and shows a 5-K warm bias in the upper stratosphere

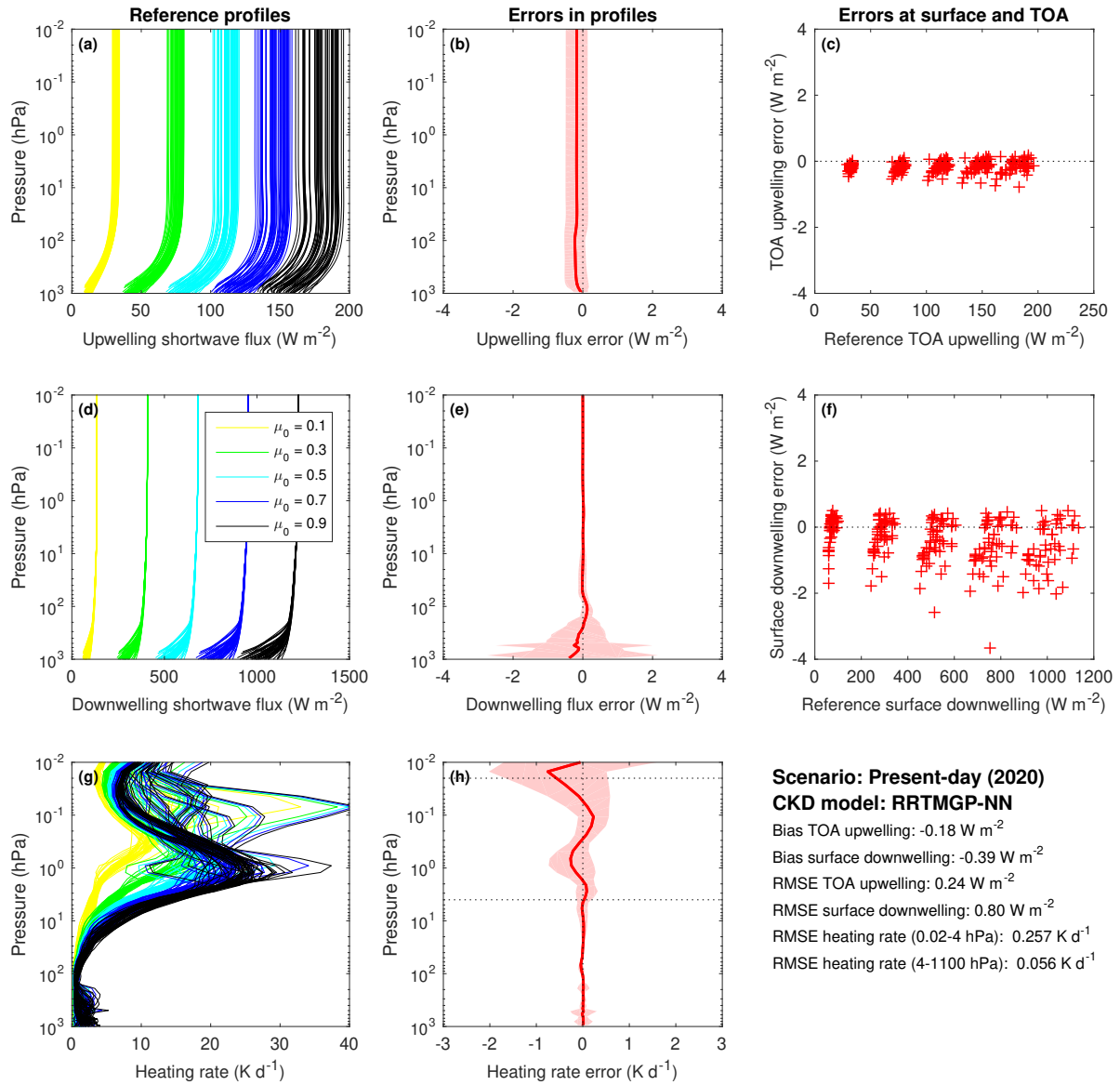
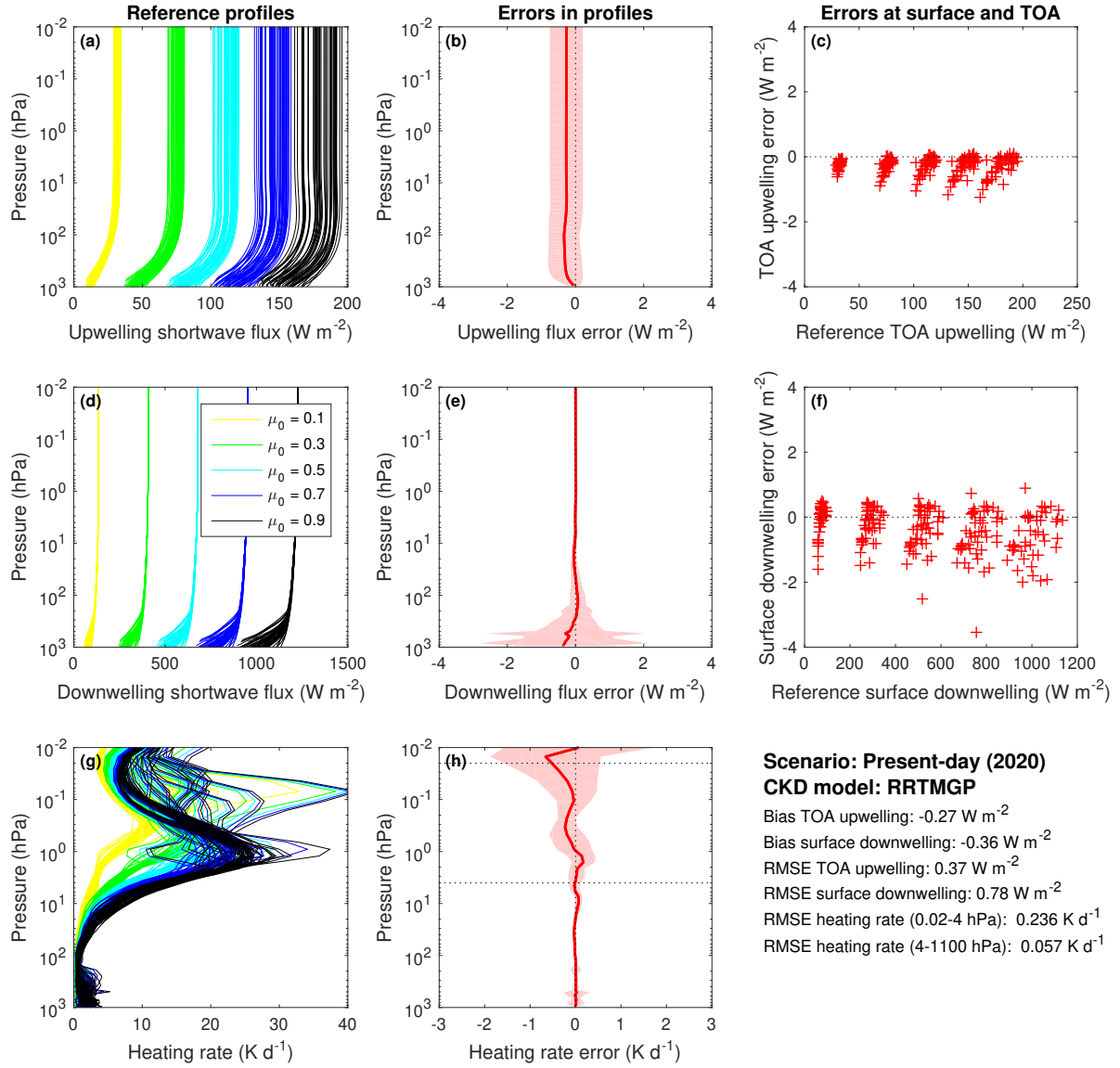


Figure 5. Evaluation of Reduced-RRTMGP-NN shortwave fluxes and heating rates using the 50 independent profiles of the CKDMIP Evaluation-1 dataset with present-day concentrations of greenhouse gases. The left column (a, d, g) shows the reference profiles of upwelling flux, downwelling flux and heating rate from LBL calculations with five different values of the cosine of the solar zenith angle, μ_0 (0.1, 0.3, 0.5, 0.7 and 0.9). The middle column (b, e, h) shows the corresponding biases (solid lines) and 95th percentile of errors (shaded area) using all 250 data points. The right column (c, f) depicts instantaneous errors in upwelling TOA and downwelling surface fluxes with the clusters corresponding to the different solar zenith angles.



Scenario: Present-day (2020)
CKD model: RRTMGP

Bias TOA upwelling: -0.27 W m^{-2}
 Bias surface downwelling: -0.36 W m^{-2}
 RMSE TOA upwelling: 0.37 W m^{-2}
 RMSE surface downwelling: 0.78 W m^{-2}
 RMSE heating rate (0.02-4 hPa): 0.236 K d^{-1}
 RMSE heating rate (4-1100 hPa): 0.057 K d^{-1}

Figure 6. As in Fig. 5 but for Reduced-RRTMGP.

for RRTMG, and larger in the mesosphere. The same bias was reported by Hogan et al. (2017), which they explained by the use of the older ‘Kurucz’ solar spectrum in the RRTMG version used in ecRad. RRTMGP uses a more recent solar spectrum with less ultraviolet radiation, resulting in closer agreement with MLS. In the mesosphere, RRTMGP-NN is much closer to the Reduced-RRTMGP scheme than Reduced-RRTMGP is to Full-RRTMGP (Fig. 8 (c)). This strongly suggests that the emulation errors are small enough to be acceptable.

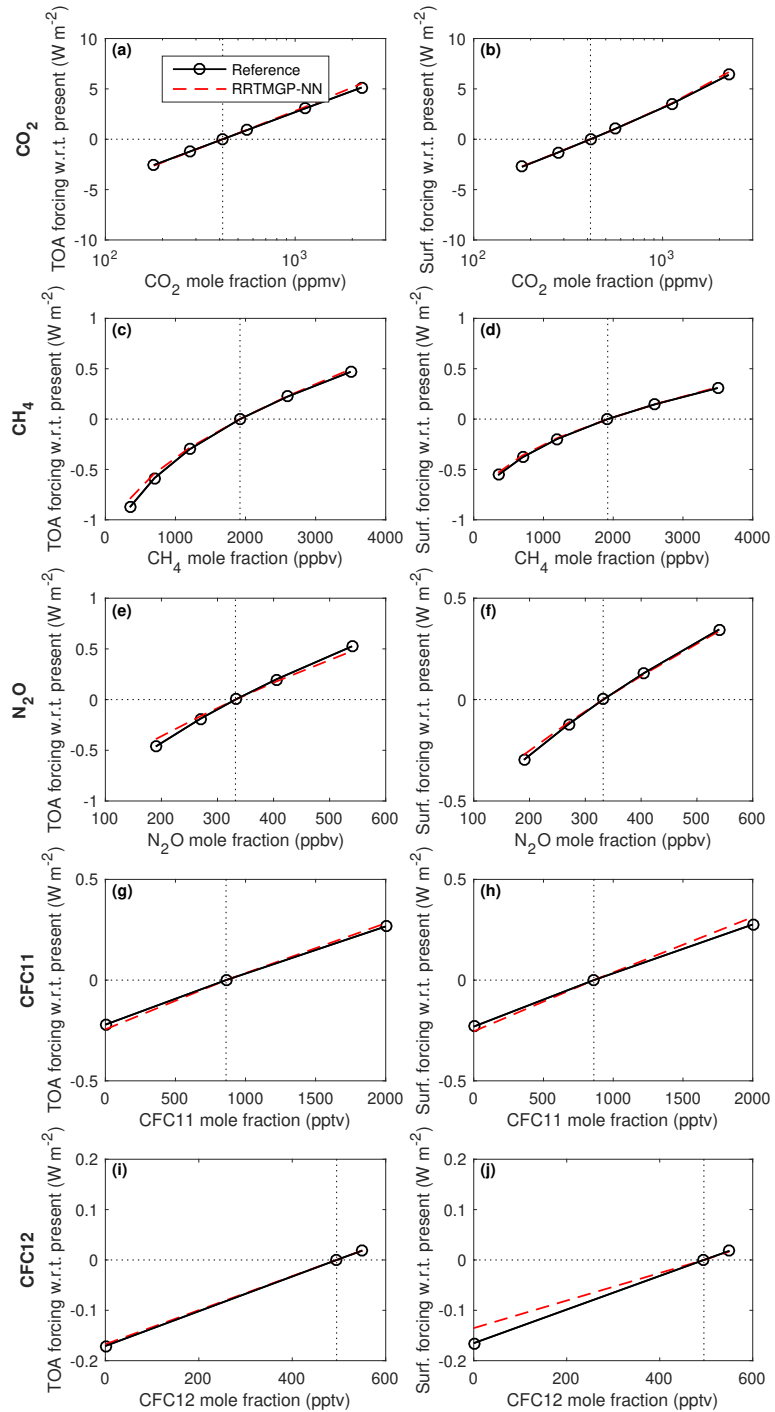


Figure 7. Comparison of RRTMGP-NN and LBL calculations of instantaneous longwave clear-sky radiative forcing at top of atmosphere (left column) and surface (right column) when perturbing different greenhouse gases (rows), averaged over the 50 Evaluation 1 profiles.

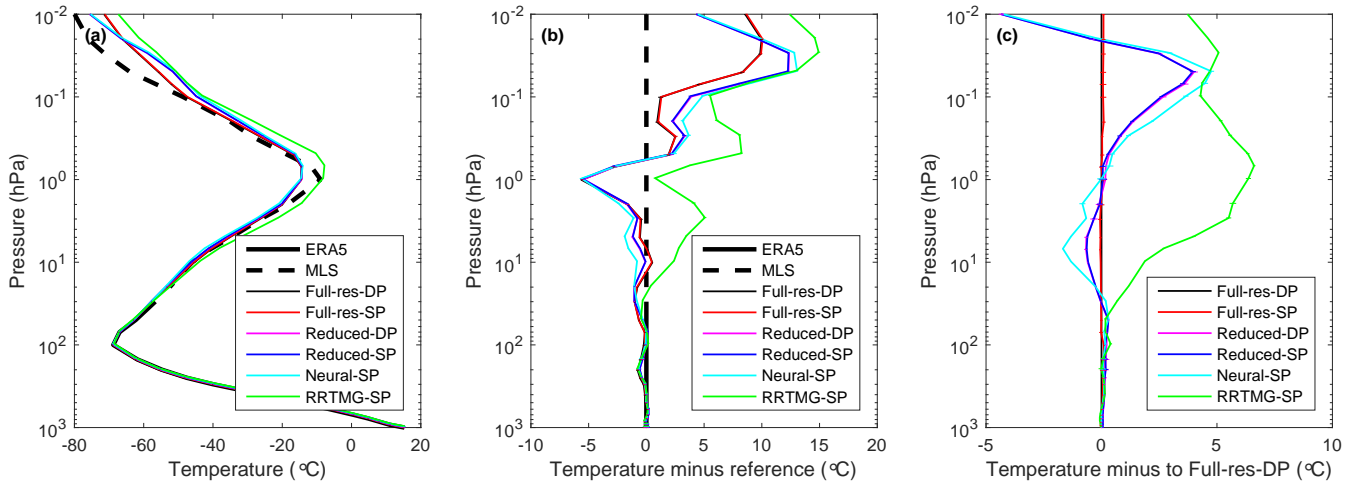


Figure 8. Evaluation of global/annual-mean temperature profiles from free-running simulations by the IFS. (a) Mean temperature, (b) difference against a reference dataset consisting of the MLS climatology above the 20-hPa height level and ERA5 below this level, and (c) difference against a simulation using full-resolution RRTMGP in double precision. The small horizontal bars give the 95% confidence interval as computed from differences between different years. As indicated in the legend, the simulations were performed in double or single precision (DP or SP) using the full- or reduced-resolution RRTMGP, the NN emulation of (reduced-)RRTMGP, or the older RRTMGP gas optics scheme.

A height-latitude cross section of temperature likewise shows larger differences between the old RRTMGP scheme and RRTMGP than between different RRTMGP configurations and the NN version (Fig. 9). A strong warm bias in the stratosphere is evident for RRTMGP but less so for any version of RRTMGP, although the RRTMGP(-NN) runs do show a weaker upper-stratospheric warm bias over high latitudes and a substantial cold bias in the tropical stratosphere.

Finally, Fig. 10 compares annual/zonal means of 2-m temperature, TOA net LW and SW fluxes, and downwelling SW flux between simulations using different gas optics configurations. In general the differences relative to Full-RRTMGP are statistically insignificant as the means fall within the error bars computed from the 4-year sample. The only clear exception is RRTMGP, which, for instance, at lower latitudes has significantly larger surface downwelling SW flux and smaller LW flux than Full-RRTMGP. These findings are consistent in sign and approximate magnitude with the evaluation of RRTMGP against line-by-line calculations by Hogan and Matricardi (2020), although it should be stressed that these differences of 0–2 W m⁻² are still very modest.

370 5 Conclusions

In this paper we have evaluated RRTMGP-NN, a neural network version of the RRTMGP gas optics scheme, integrated into ECMWF's radiation scheme ecRad, by performing both offline calculations and four 1-year simulations with the free-running IFS model. Emulating only the gas optics component, instead of the full radiation scheme like in previous work, results in much

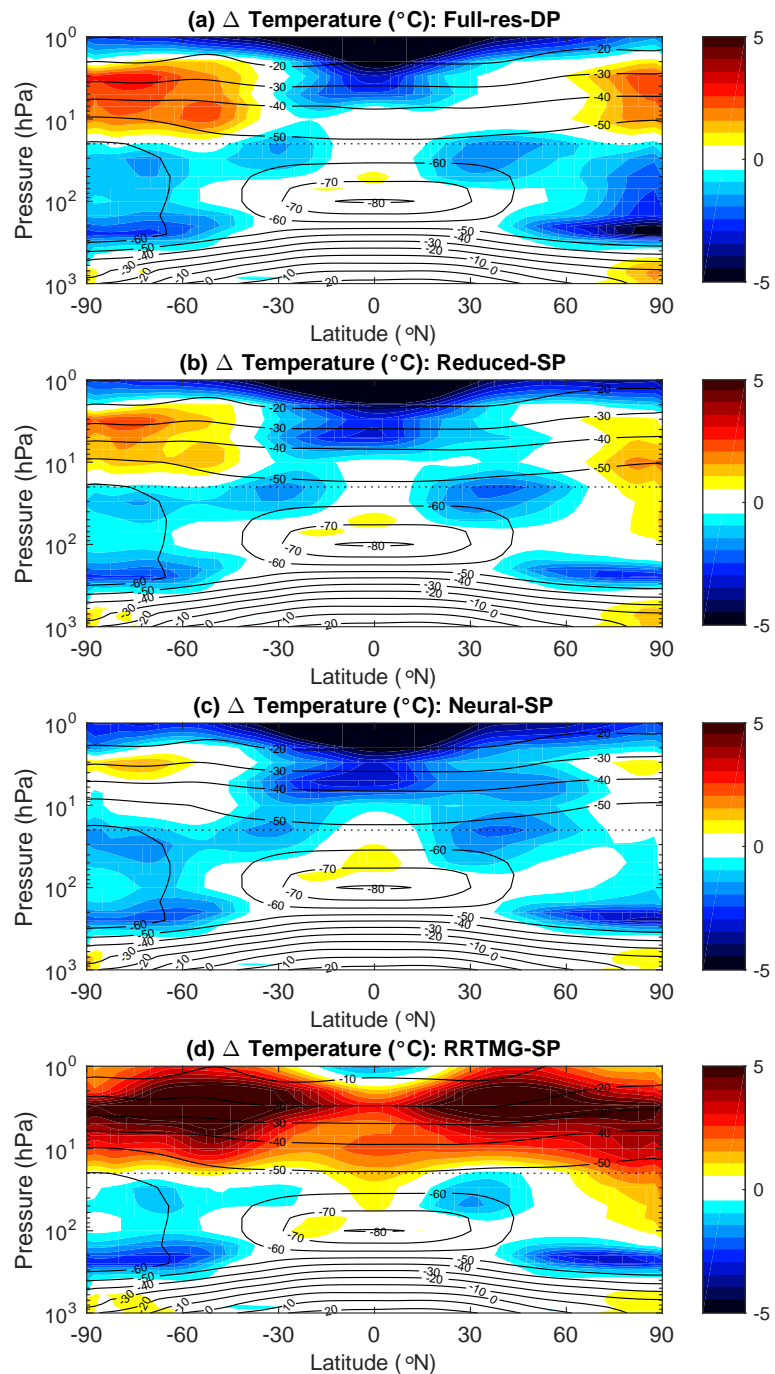


Figure 9. Similar to Fig. 8 but showing the height-latitude cross section of mean temperature (black contours) and temperature difference (colors) against the reference datasets, and only until 1 hPa.

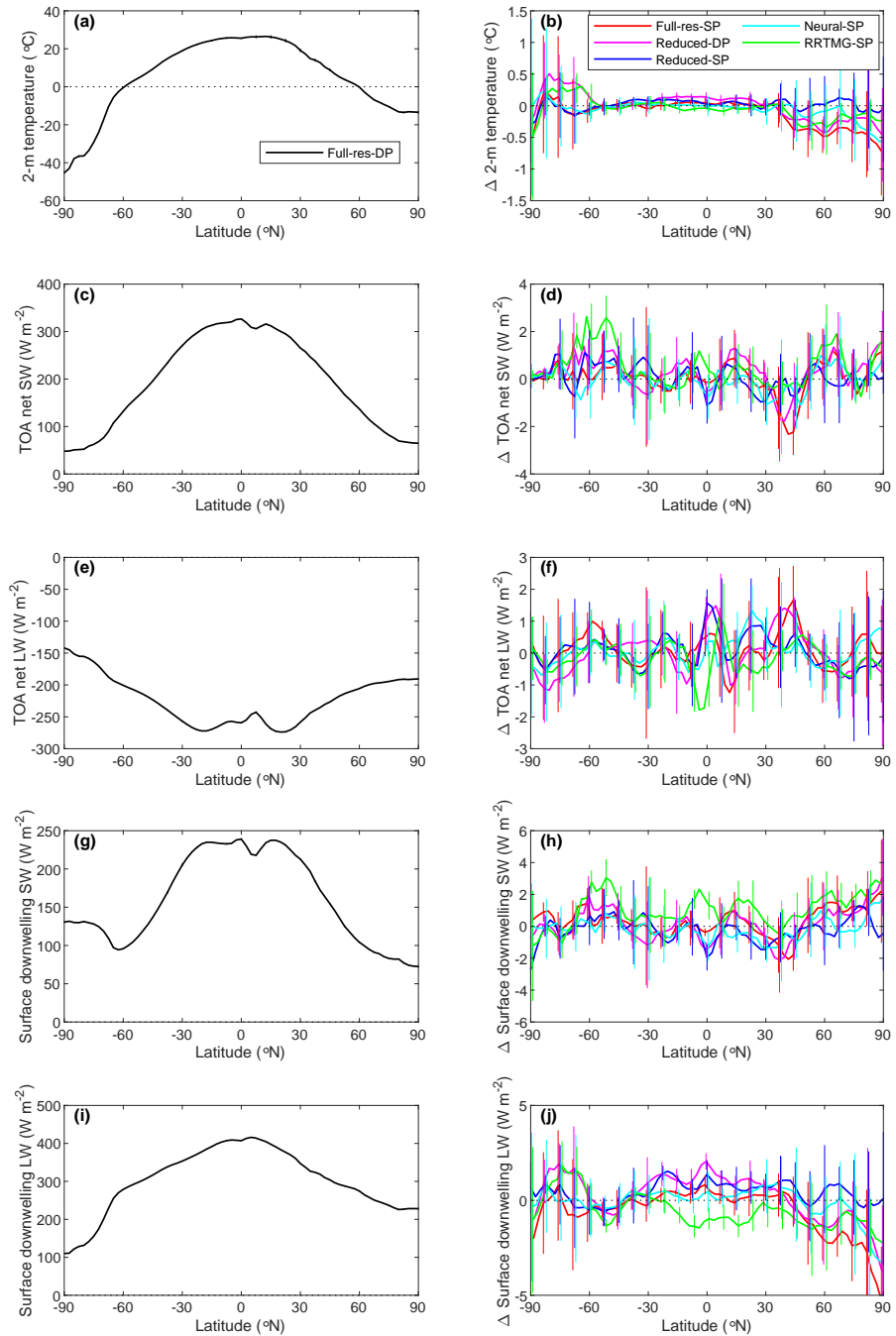


Figure 10. Zonal mean of different single-level quantities using the reference Full-RRTMGP run in double precision (a, c, e, g, i) and differences relative to this run (b, d, f, h, j) with the vertical lines indicating the 95% confidence interval: (a, b) 2-m temperature, (c, d) TOA net SW flux, (e, f) TOA net LW flux, (g, h) surface downwelling SW flux, and (i, j) surface downwelling LW flux.

375 better accuracy. The NNs were trained on diverse datasets which cover a wide range of gas concentrations and atmospheric
376 conditions (including pre-industrial, present-day and future conditions). Although training on optical properties derived from
377 RRTMGP, we used early-stopping with respect to a validation set containing broadband fluxes computed by a line-by-line
378 model, based on metrics which included radiative forcings. Combining this with the use of a hybrid loss function, we were able
379 to reduce radiative forcing errors. Clear-sky shortwave and longwave fluxes, heating rates, and top-of-atmosphere and surface
380 forcings for 5 greenhouse gases were evaluated against line-by-line computations using an independent dataset spanning a
381 wide range of climate scenarios. In each case, any emulation errors introduced by RRTMGP-NN were virtually undetectable
382 compared to the parameterization error. Both schemes have heating rate errors within 0.056-0.057 K d⁻¹ (SW) and 0.102-0.116
383 K d⁻¹ (LW). Flux errors were generally below 1 W m⁻² and upwelling fluxes were actually improved by using RRTMGP-NN.
384 Fluxes for cloudy profiles would be even less affected as the treatment of clouds is identical in our approach.

385 The results from the online evaluation are also highly encouraging as they show very similar model climates for RRT-
386 MGP and RRTMGP-NN. Global/annual mean temperature profiles for the reduced-spectral-resolution RRTMGP and its NN
387 emulator are in closer agreement than different versions of RRTMGP are to each other, and all of these schemes, including
388 RRTMGP-NN, substantially reduce stratosphere and mesosphere temperature biases relative to the older RRTMG scheme. In
389 single-level fields, the differences between RRTMGP-NN and RRTMGP are obscured by natural variability. These results,
390 taken together with those from the offline evaluation, demonstrate that our RRTMGP-NN models are safe and suitable for
391 operational weather and climate models. To our knowledge, the same has not been demonstrated for full radiation scheme em-
392 ululators, whose substantial emulation errors particularly for cloudy profiles (Fig. 2, Song and Roh, 2021), and potential lack of
393 reliability and energy conservation, is especially worrisome for climate modeling applications. For instance, radiative forcings
394 with respect to greenhouse gases, or cloud radiative effects, have not been evaluated in any emulator study we are aware of. We
395 would also highlight the advantages of modular radiation schemes, which allows reducing model uncertainties in a continuous
396 and interpretable manner by developing new and improved solvers, gas, aerosol or cloud optics schemes independently of one
397 another.

400 Our evaluation of RRTMGP-NN was based on a setup with a reduced set of LW gases (using artificially increased CFC-11
401 concentrations to represent further gases); for applications where the individual radiative forcings of other RRTMGP minor
402 greenhouse gases are of importance, such metrics can be evaluated offline and new NN models trained if needed. The data
403 and tools are freely available and may be useful for future work. We encourage developers of new gas optics schemes to
404 consider NNs as part of their toolbox, as they combine computational efficiency with algorithmic flexibility that allows avoiding
405 structural assumptions, although training multi-gas models directly on line-by-line data could be challenging in terms of data
406 generation and optimizing for minor gases.

407 In offline timings obtained on ECMWF's AMD-based supercomputer, using RRTMGP-NN instead of RRTMGP makes
408 ecRad 1.5 times faster. This should be a significant reduction especially for climate models, which can spend a large share
409 of the total model runtime on radiation. For instance, in coarse-resolution simulations using the ECHAM climate model, it
410 accounted for half of the runtime of the atmospheric model (Cotronei and Slawig, 2020). (In the IFS, radiation is currently only
411 a few percent of the model runtime but this is largely due to it being called on a coarser grid and only every hour). While studies

emulating the entire radiation scheme have reported much larger speed-ups of 1–2 orders of magnitude, comparisons are often
410 against old and slow radiation codes (e.g. Lagerquist et al., 2021), and gains may be much smaller against state-of-the-art
schemes. For instance, by combining performance refactoring (that we plan to describe in a future paper) with algorithmic
415 developments that allow reducing the spectral dimension (Hogan and Maticardi, 2022), the cost of ecRad with TripleClouds
is reduced by an order of magnitude compared to the operational version using McICA (Hogan and Bozzo, 2018), which was
already significantly faster than the previous ECMWF radiation scheme. Adopting common metrics for efficiency (e.g. time per
420 column per CPU core) and accuracy, and standard datasets for independent verification, would no doubt be helpful for getting a
clearer view of the usefulness of radiation emulators. Unfortunately, the latter may be difficult in practice given limitations such
as inflexibility with regards to the vertical grid, which affect usual emulation approaches. Nevertheless, as machine learning
does not offer a magic bullet to the accuracy/speed trade-off problem (Ukkonen, 2022a), it is important that both are carefully
425 evaluated in emulator studies.

420 *Code and data availability.* RTE+RRTMGP-NN is available on Github (<https://github.com/peterukk/rte-rrtmgp-nn>); the Fortran programs
and Python scripts used for data generation and model training are found in the /examples/rrtmgp-nn-training subdirectory. The archived
RTE-RRTMGP-NN 2.0 version and training data has also been uploaded to Zenodo (<https://doi.org/10.5281/zenodo.6576680>), as has the
optimized non-official version of ecRad integrated with RRTMGP-NN 2.0 (<https://doi.org/10.5281/zenodo.7148329>).

Appendix A: CKDMIP evaluation for the longwave

425 This section contains longwave results for the RRTMGP gas optics model with reduced spectral resolution (Reduced-RRTMGP),
and its neural network (NN) version, using the experiment protocol, data and tools from the Correlated K-Distribution Model
Intercomparison Project (CKDMIP). Four figures are included, corresponding to different gas optics models and gas concen-
tration scenarios: RRTMGP-NN, present-day (Fig. A1), RRTMGP, present-day (Fig. A2), RRTMGP-NN, future (Fig. A3), and
430 RRTMGP, future (Fig. A4). The calculations were performed using a no-scattering solver with four discrete zenith angles in
each hemisphere.

Author contributions. The conceptualization of the paper was mostly by PU. The machine learning work, including model design and data
generation, was carried out by PU. Implementation of RRTMGP-NN in ecRad was done by PU but with input from RJH. Both authors
contributed to the offline evaluation (timings by PU). The IFS experiments were mostly designed by RJH and carried out by PU. PU prepared
the manuscript with contributions from RJH.

435 *Competing interests.* No competing interests are present.

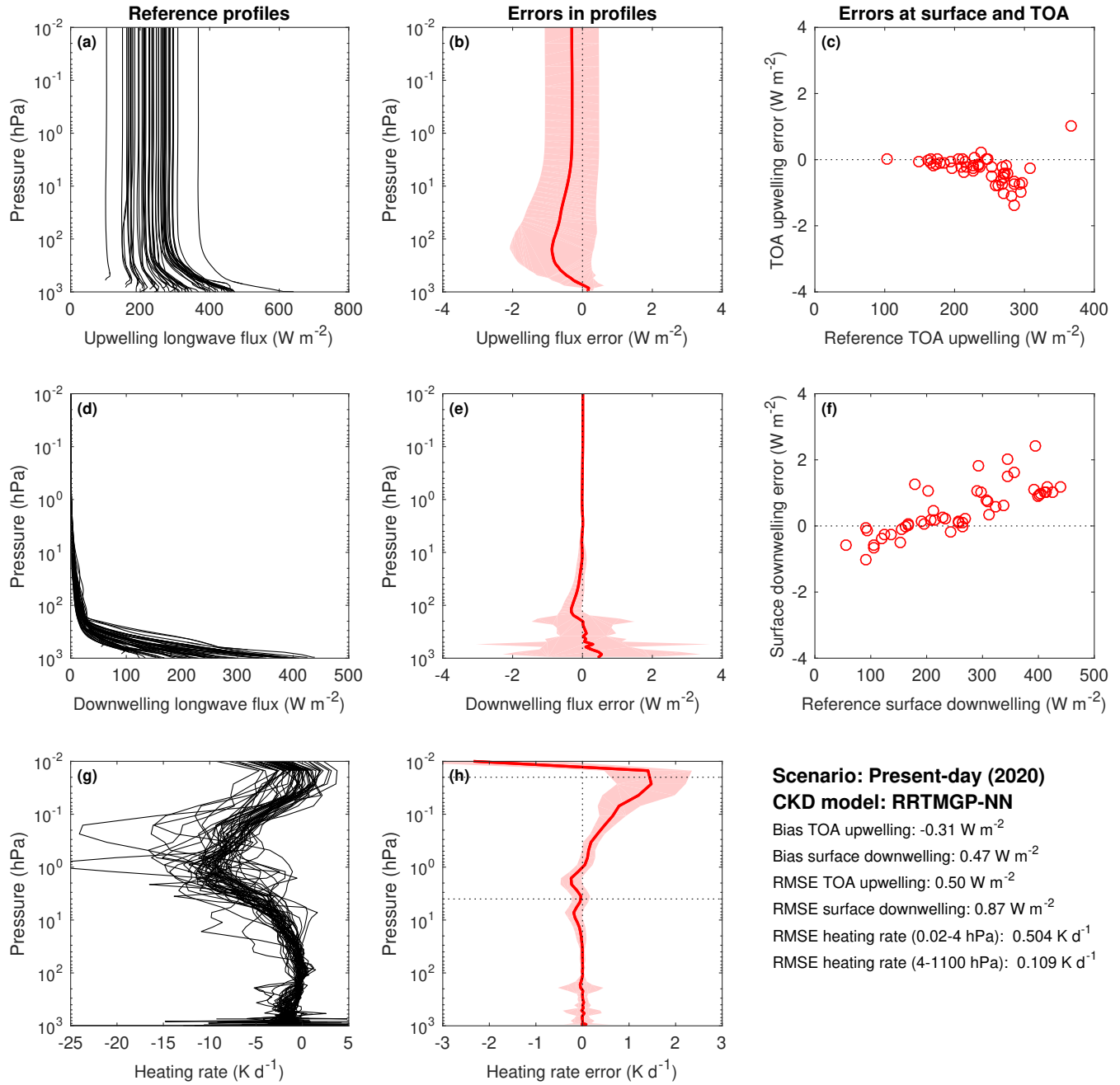


Figure A1. Evaluation of Reduced-RRTMGP-NN longwave fluxes and heating rates using the 50 independent profiles of the CKDMIP Evaluation-1 dataset with present-day concentrations of greenhouse gases. Reference profiles of upwelling, downwelling flux and heating rate from LBL calculations, corresponding errors (b, e, h) with solid lines showing bias and the shaded area giving the 95th percentile of errors, and instantaneous errors in upwelling TOA and downwelling surface fluxes (c, f).

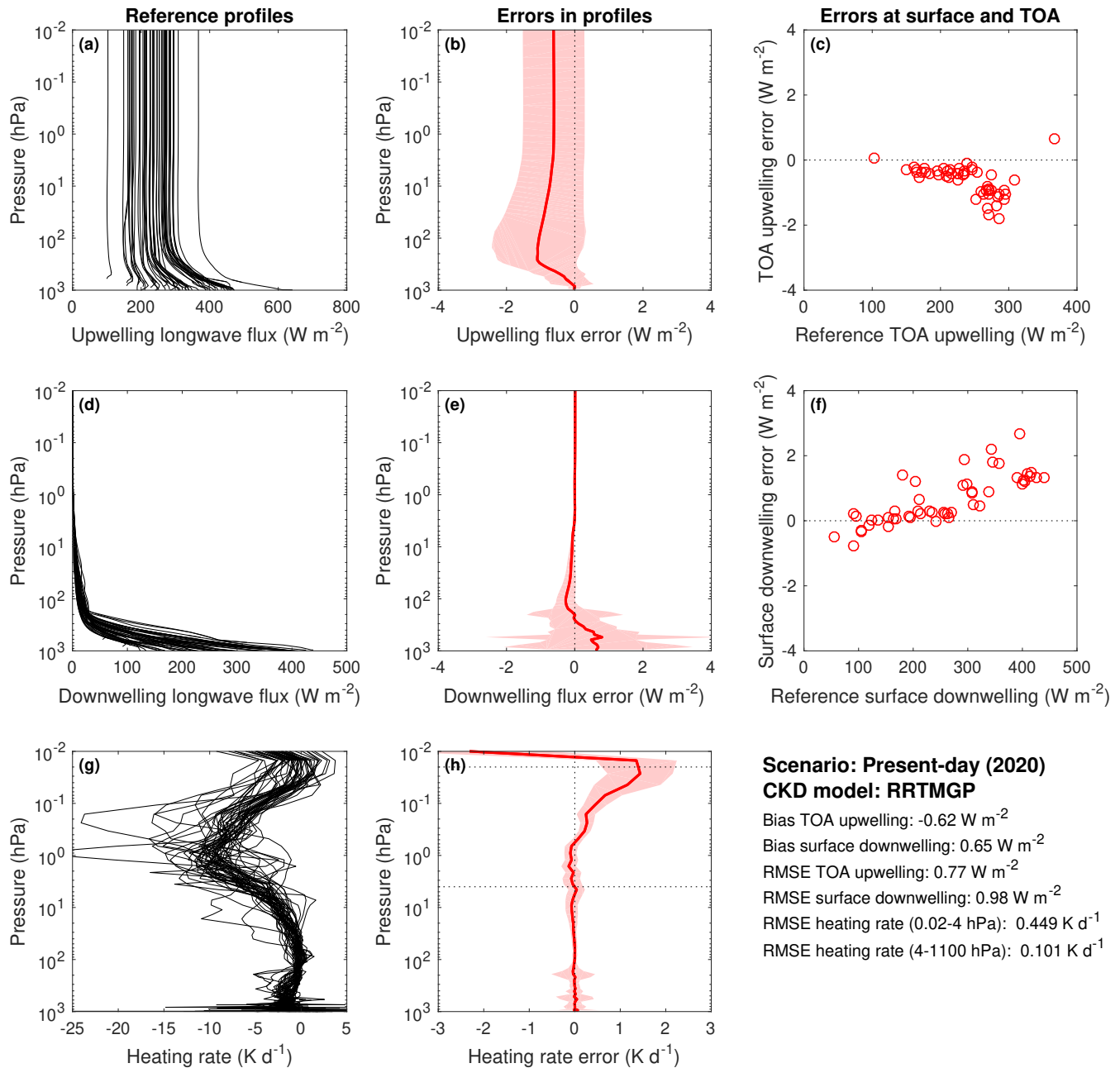


Figure A2. As in Fig. A1 but for the original Reduced-RRTMGP.

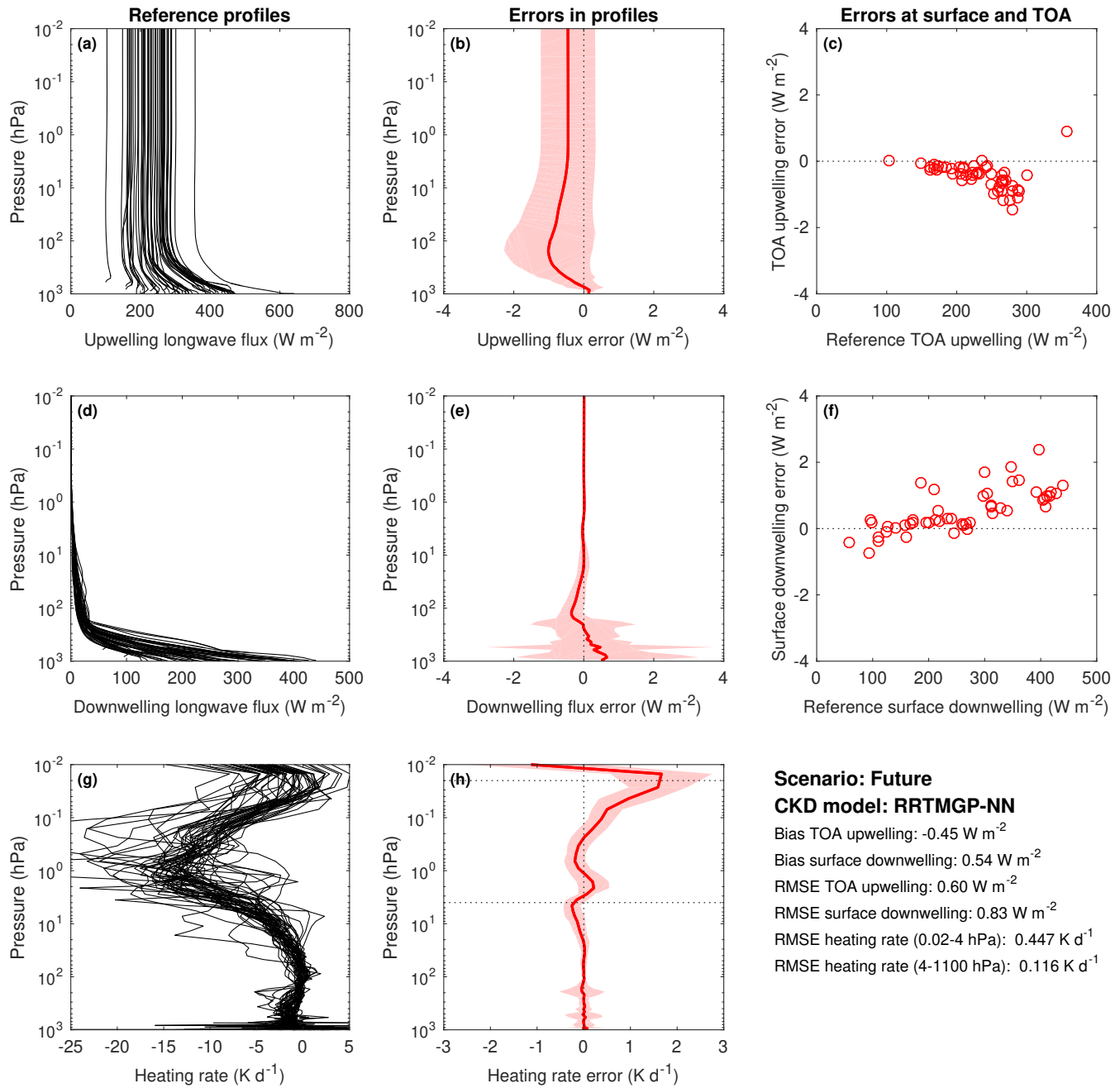


Figure A3. As in Fig. A1 but for the future scenario.

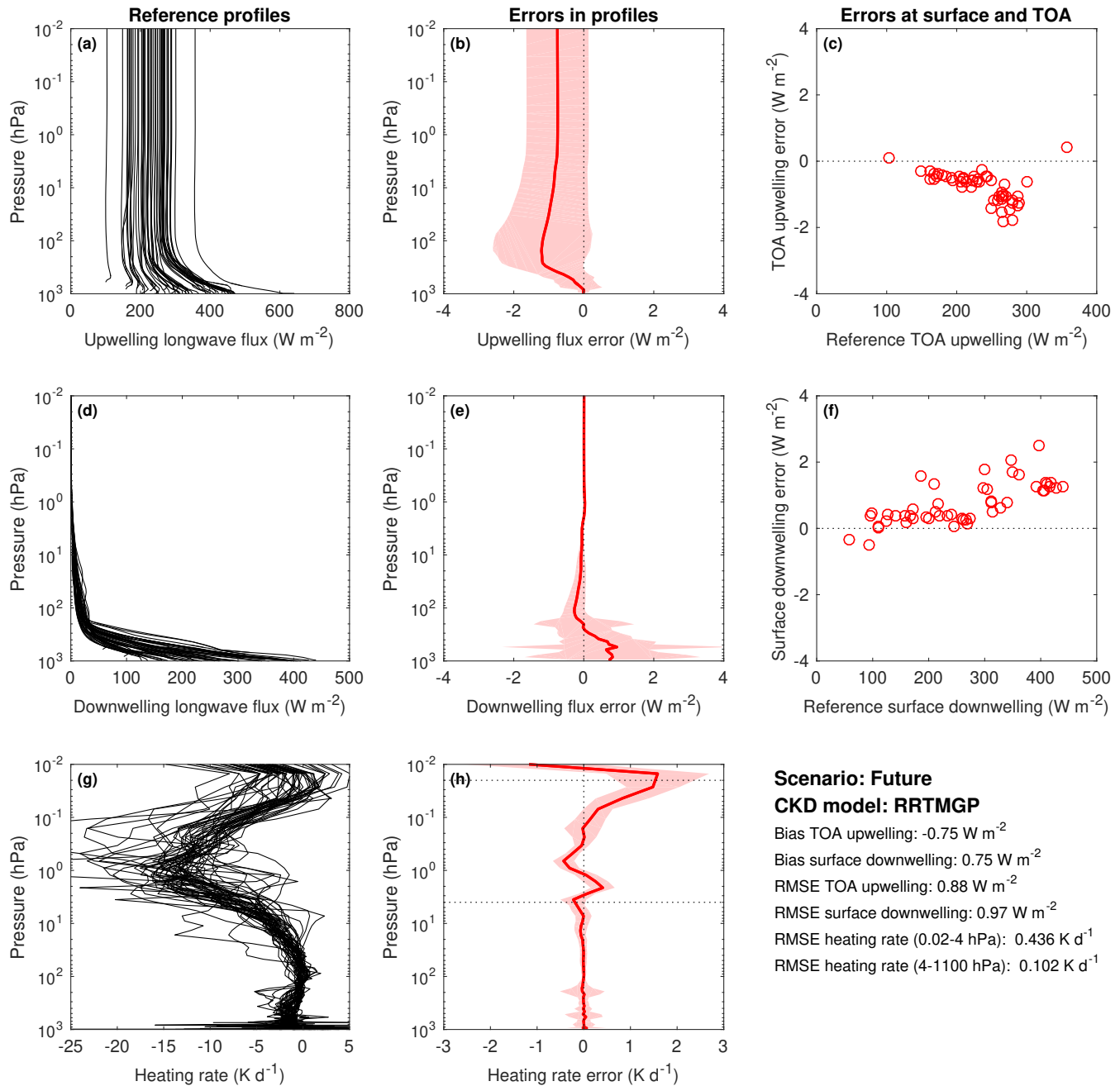


Figure A4. As in Fig. A1 but for the future scenario and Reduced-RRTMGP.

Acknowledgements. The authors thank Robert Pincus, and the two anonymous reviewers, for reading the manuscript and providing useful suggestions to improve its clarity.

References

Bradbury, J., Frostig, R., Hawkins, P., Johnson, M. J., Leary, C., Maclaurin, D., Necula, G., Paszke, A., VanderPlas, J., Wanderman-Milne,
440 S., and Zhang, Q.: JAX: composable transformations of Python+NumPy programs, <http://github.com/google/jax>, 2018.

Brenowitz, N. D. and Bretherton, C. S.: Prognostic validation of a neural network unified physics parameterization, *Geophysical Research Letters*, 45, 6289–6298, <https://doi.org/10.1029/2018gl078510>, 2018.

Brenowitz, N. D., Beucler, T., Pritchard, M., and Bretherton, C. S.: Interpreting and stabilizing machine-learning parametrizations of convection, *Journal of the Atmospheric Sciences*, 77, 4357–4375, 2020.

445 Chevallier, F., Chéruy, F., Scott, N., and Chédin, A.: A neural network approach for a fast and accurate computation of a longwave radiative budget, *Journal of applied meteorology*, 37, 1385–1397, 1998.

Cotronei, A. and Slawig, T.: Single-precision arithmetic in ECHAM radiation reduces runtime and energy consumption, *Geoscientific Model Development*, 13, 2783–2804, 2020.

Curcic, M.: A parallel Fortran framework for neural networks and deep learning, in: ACM SIGPLAN Fortran Forum, vol. 38, pp. 4–21, ACM
450 New York, NY, USA, 2019.

Garand, L., Turner, D., Larocque, M., Bates, J., Boukabara, S., Brunel, P., Chevallier, F., Deblonde, G., Engelen, R., Hollingshead, M., et al.: Radiance and Jacobian intercomparison of radiative transfer models applied to HIRS and AMSU channels, *Journal of Geophysical Research: Atmospheres*, 106, 24 017–24 031, 2001.

Gentine, P., Pritchard, M., Rasp, S., Reinaudi, G., and Yacalis, G.: Could machine learning break the convection parameterization deadlock?,
455 *Geophysical Research Letters*, 45, 5742–5751, <https://doi.org/10.1029/2018gl078202>, 2018.

Goody, R., West, R., Chen, L., and Crisp, D.: The correlated-k method for radiation calculations in nonhomogeneous atmospheres, *Journal of Quantitative Spectroscopy and Radiative Transfer*, 42, 539–550, 1989.

Hogan, R. J. and Bozzo, A.: A flexible and efficient radiation scheme for the ECMWF model, *Journal of Advances in Modeling Earth Systems*, 10, 1990–2008, <https://doi.org/10.1029/2018MS001364>, 2018.

460 Hogan, R. J. and Matricardi, M.: Evaluating and improving the treatment of gases in radiation schemes: the Correlated K-Distribution Model Intercomparison Project (CKDMIP), *Geoscientific Model Development Discussions*, 2020, 1–29, <https://doi.org/10.5194/gmd-2020-99>, 2020.

Hogan, R. J. and Matricardi, M.: A tool for generating fast k-distribution gas-optics models for weather and climate applications, *Earth and Space Science Open Archive*, p. 24, <https://doi.org/10.1002/essoar.10510456.1>, 2022.

465 Hogan, R. J., Schäfer, S. A., Klinger, C., Chiu, J. C., and Mayer, B.: Representing 3-D cloud radiation effects in two-stream schemes: 2. Matrix formulation and broadband evaluation, *Journal of Geophysical Research: Atmospheres*, 121, 8583–8599, 2016.

Hogan, R. J., Ahlgrimm, M., Balsamo, G., Beljaars, A., Berrisford, P., Bozzo, A., Di Giuseppe, F., Forbs, R. M., Haiden, T., Lang, S., Mayer, M., Polichtchouk, I., Sandu, I., Vitart, V., and Wedi, N.: Radiation in numerical weather prediction, *Tech. Memo. 816*, ECMWF, 2017.

Iacono, M. J., Mlawer, E. J., Clough, S. A., and Morcrette, J.-J.: Impact of an improved longwave radiation model, RRTM, on the energy
470 budget and thermodynamic properties of the NCAR community climate model, CCM3, *Journal of Geophysical Research: Atmospheres*, 105, 14 873–14 890, 2000.

Inness, A., Ades, M., Agusti-Panareda, A., Barré, J., Benedictow, A., Blechschmidt, A.-M., Dominguez, J., Engelen, R., Eskes, H., Flemming, J., et al.: The CAMS reanalysis of atmospheric composition, *Atmospheric Chemistry and Physics*, 19, 3515–3556, 2019.

475 Krasnopolksy, V., Fox-Rabinovitz, M., Hou, Y., Lord, S., and Belochitski, A.: Accurate and fast neural network emulations of model radiation for the NCEP coupled climate forecast system: climate simulations and seasonal predictions, *Monthly Weather Review*, 138, 1822–1842, 2010.

Krasnopolksy, V. M., Fox-Rabinovitz, M. S., and Belochitski, A. A.: Decadal climate simulations using accurate and fast neural network emulation of full, longwave and shortwave, radiation, *Monthly Weather Review*, 136, 3683–3695, 2008.

480 Lagerquist, R., Turner, D., Ebert-Uphoff, I., Stewart, J., and Hagerty, V.: Using Deep Learning to Emulate and Accelerate a Radiative Transfer Model, *Journal of Atmospheric and Oceanic Technology*, 38, 1673–1696, 2021.

Liu, Y., Caballero, R., and Monteiro, J. M.: RadNet 1.0: Exploring deep learning architectures for longwave radiative transfer, *Geoscientific Model Development*, 13, 4399–4412, 2020.

485 Meinshausen, M., Vogel, E., Nauels, A., Lorbacher, K., Meinshausen, N., Etheridge, D. M., Fraser, P. J., Montzka, S. A., Rayner, P. J., Trudinger, C. M., et al.: Historical greenhouse gas concentrations for climate modelling (CMIP6), *Geoscientific Model Development*, 10, 2057–2116, 2017.

Mlawer, E. J., Taubman, S. J., Brown, P. D., Iacono, M. J., and Clough, S. A.: Radiative transfer for inhomogeneous atmospheres: RRTM, a validated correlated-k model for the longwave, *Journal of Geophysical Research: Atmospheres*, 102, 16 663–16 682, 1997.

Pal, A., Mahajan, S., and Norman, M. R.: Using Deep Neural Networks as Cost-Effective Surrogate Models for Super-Parameterized E3SM Radiative Transfer, *Geophysical Research Letters*, 46, 6069–6079, [https://doi.org/https://doi.org/10.1029/2018GL081646](https://doi.org/10.1029/2018GL081646), 2019.

490 Pincus, R., Forster, P. M., and Stevens, B.: The Radiative Forcing Model Intercomparison Project (RFMIP): experimental protocol for CMIP6, *Geoscientific Model Development*, 9, 3447–3460, <https://doi.org/10.5194/gmd-9-3447-2016>, 2016.

Pincus, R., Mlawer, E. J., and Delamere, J. S.: Balancing accuracy, efficiency, and flexibility in radiation calculations for dynamical models, *Journal of Advances in Modeling Earth Systems*, 11, 3074–3089, [https://doi.org/https://doi.org/10.1029/2019MS001621](https://doi.org/10.1029/2019MS001621), 2019.

Rasp, S., Pritchard, M. S., and Gentine, P.: Deep learning to represent subgrid processes in climate models, *Proceedings of the National 495 Academy of Sciences*, 115, 9684–9689, <https://doi.org/10.1073/pnas.1810286115>, 2018.

Roh, S. and Song, H.-J.: Evaluation of neural network emulations for radiation parameterization in cloud resolving model, *Geophysical Research Letters*, 47, e2020GL089444, [https://doi.org/https://doi.org/10.1029/2020GL089444](https://doi.org/10.1029/2020GL089444), 2020.

Shonk, J. K. and Hogan, R. J.: Tripleclouds: An efficient method for representing horizontal cloud inhomogeneity in 1D radiation schemes by using three regions at each height, *Journal of Climate*, 21, 2352–2370, 2008.

500 Song, H.-J. and Roh, S.: Improved weather forecasting using neural network emulation for radiation parameterization, *Journal of Advances in Modeling Earth Systems*, 13, e2021MS002609, [https://doi.org/https://doi.org/10.1029/2021MS002609](https://doi.org/10.1029/2021MS002609), 2021.

Ukkonen, P.: Exploring pathways to more accurate machine learning emulation of atmospheric radiative transfer, *Journal of Advances in Modeling Earth Systems*, p. e2021MS002875, <https://doi.org/10.1029/2021MS002875>, 2022a.

Ukkonen, P.: Improving the trade-off between accuracy and efficiency of atmospheric radiative transfer computations by using machine learning and code optimization, Ph.D. thesis, School of The Faculty of Science, University of Copenhagen, 2022b.

505 Ukkonen, P., Pincus, R., Hogan, R. J., Nielsen, K. P., and Kaas, E.: Accelerating radiation computations for dynamical models with targeted machine learning and code optimization, *Journal of Advances in Modeling Earth Systems*, 12, e2020MS002226, [https://doi.org/https://doi.org/10.1029/2020MS002226](https://doi.org/10.1029/2020MS002226), 2020.

Veerman, M. A., Pincus, R., Stoffer, R., Van Leeuwen, C. M., Podareanu, D., and Van Heerwaarden, C. C.: Predicting atmospheric optical properties for radiative transfer computations using neural networks, *Philosophical Transactions of the Royal Society A*, 379, 20200095, 2021.

Wang, X., Han, Y., Xue, W., Yang, G., and Zhang, G. J.: Stable climate simulations using a realistic general circulation model with neural network parameterizations for atmospheric moist physics and radiation processes, *Geoscientific Model Development*, 15, 3923–3940, 2022.

515 Yuval, J., O'Gorman, P. A., and Hill, C. N.: Use of neural networks for stable, accurate and physically consistent parameterization of subgrid atmospheric processes with good performance at reduced precision, *Geophysical Research Letters*, 48, e2020GL091363, <https://doi.org/https://doi.org/10.1029/2020GL091363>, 2021.